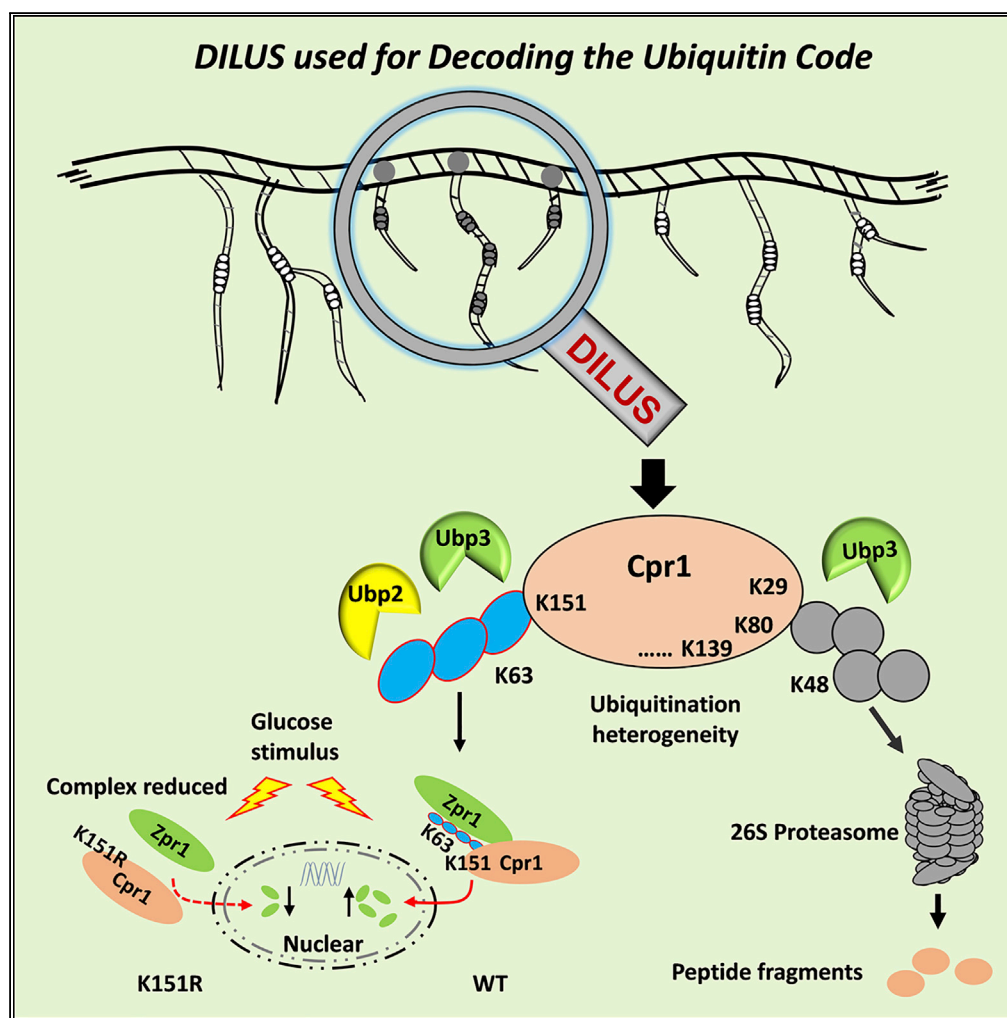


## Article

# Ubiquitin Linkage Specificity of Deubiquitinases Determines Cyclophilin Nuclear Localization and Degradation



Yanchang Li,  
Qiuyan Lan, Yuan  
Gao, ..., Fuchu He,  
Daniel Finley, Ping  
Xu

xuping@mail.ncpsb.org

#### HIGHLIGHTS

Quantitative proteomics is used to reflect DUB's linkage specificity *in vivo*

DILUS is developed to decode the ubiquitin code on the level of ubiquitinated sites

K63 chains on K151 of Cpr1 regulated by Ubp2/ Ubp3 mediates Zpr1's nuclear transition

K48 chains on non-K151 of Cpr1 regulated by Ubp3 controls its proteasomal proteolysis

#### DATA AND CODE

#### AVAILABILITY

PXD017357

Li et al., iScience 23, 100984  
April 24, 2020 © 2020 The  
Authors.  
[https://doi.org/10.1016/  
j.isci.2020.100984](https://doi.org/10.1016/j.isci.2020.100984)

## Article

# Ubiquitin Linkage Specificity of Deubiquitinases Determines Cyclophilin Nuclear Localization and Degradation

Yanchang Li,<sup>1,6</sup> Qiuyan Lan,<sup>2,6</sup> Yuan Gao,<sup>1</sup> Cong Xu,<sup>1</sup> Zhongwei Xu,<sup>1</sup> Yihao Wang,<sup>1</sup> Lei Chang,<sup>1</sup> Junzhu Wu,<sup>2</sup> Zixin Deng,<sup>2</sup> Fuchu He,<sup>1</sup> Daniel Finley,<sup>3</sup> and Ping Xu<sup>1,2,4,5,7,\*</sup>

## SUMMARY

Ubiquitin chain specificity has been described for some deubiquitinases (DUBs) but lacks a comprehensive profiling *in vivo*. We used quantitative proteomics to compare the seven lysine-linked ubiquitin chains between wild-type yeast and its 20 DUB-deletion strains, which may reflect the linkage specificity of DUBs *in vivo*. Utilizing the specificity and ubiquitination heterogeneity, we developed a method termed DUB-mediated identification of linkage-specific ubiquitinated substrates (DILUS) to screen the ubiquitinated lysine residues on substrates modified with certain chains and regulated by specific DUB. Then we were able to identify 166 Ubp2-regulating substrates with 244 sites potentially modified with K63-linked chains. Among these substrates, we further demonstrated that cyclophilin A (Cpr1) modified with K63-linked chain on K151 site was regulated by Ubp2 and mediated the nuclear translocation of zinc finger protein Zpr1. The K48-linked chains at non-K151 sites of Cpr1 were mainly regulated by Ubp3 and served as canonical signals for proteasome-mediated degradation.

## INTRODUCTION

The covalent attachment of ubiquitin onto substrate proteins is a universal eukaryotic post-translational modification (PTM) (Hershko et al., 2000). This regulatory system underlies the precise control of a broad spectrum of cellular processes including protein degradation, gene transcription, and cell cycle progression (Hoeller and Dikic, 2009; Komander and Rape, 2012). The precise regulation of cellular processes by the ubiquitin–proteasome system (UPS) relies on the substrate specificity of hundreds of UPS enzymes.

The seven lysine residues (K6, K11, K27, K29, K33, K48, and K63) and N-terminus of ubiquitin can be conjugated by other ubiquitin moieties to form eight types of chains with distinct topologies (Kulathu and Komander, 2012). There is growing evidence that ubiquitin chains bearing different linkages have distinct biological functions, referred to as the “ubiquitin code” (Komander and Rape, 2012). The two main outputs of UPS have been the protein turnover control and governance of cell signaling networks by regulation of protein localization, interactions, and activities. For example, K48-linked chain is a predominant linkage and serves as canonical signals for proteasomal degradation (Komander and Rape, 2012); K63-linked chains perform various non-degradative roles and participate in endosomal trafficking, intracellular signaling, and DNA repair (Ikeda and Dikic, 2008; Kulathu and Komander, 2012; Spence et al., 1995); K11-linked chains are involved in cell division, transcription regulation, and endoplasmic-reticulum-associated degradation (ERAD) (Li et al., 2019; Min et al., 2015; Xu et al., 2009). For atypical chains, K6-linked chain is involved in mitophagy regulation (Gersch et al., 2017); K27-linked chains act as recruiting proteins for DNA repair and immune response (Wang et al., 2014); K33-linked chains have been implicated in cell-surface-receptor-mediated immunity, signal transduction, and protein trafficking (Huang et al., 2010; Yuan et al., 2014). In addition, branched ubiquitin chains and ubiquitin with other PTMs have been recently recognized (Stolz and Dikic, 2018). This diversity of function reflects the varieties of the ubiquitin chain structures that are specifically recognized by ubiquitin receptors (Husnjak and Dikic, 2012; Kulathu and Komander, 2012).

The formation of ubiquitin chains is regulated by ubiquitin-conjugating enzymes (E2s) and ubiquitin ligases (E3s) (Chen et al., 2019; Finley et al., 2012), whereas the detachment of ubiquitination is mediated by deubiquitinating enzymes (DUBs) (Clague et al., 2019). To date, 21 and approximately 100 DUBs have

<sup>1</sup>State Key Laboratory of Proteomics, Beijing Proteome Research Center, National Center for Protein Sciences (Beijing), Research Unit of Proteomics & Research and Development of New Drug of Chinese Academy of Medical Sciences, Beijing Institute of Lifeomics, 38 Science Park Road, Beijing 102206, China

<sup>2</sup>School of Basic Medical Science, Key Laboratory of Combinatorial Biosynthesis and Drug Discovery of Ministry of Education, School of Pharmaceutical Sciences, Wuhan University, Wuhan 430071, China

<sup>3</sup>Department of Cell Biology, Harvard Medical School, Boston, MA 02115, USA

<sup>4</sup>Guizhou University School of Medicine, Guiyang 550025, China

<sup>5</sup>Second Clinical Medicine Collage, Guangzhou University Chinese Medicine, Guangzhou 510006, China

<sup>6</sup>These authors contributed equally

<sup>7</sup>Lead Contact

\*Correspondence: xuping@mail.ncpsb.org

<https://doi.org/10.1016/j.isci.2020.100984>



been identified in the genomes of *S. cerevisiae* and humans, respectively (Abdul Rehman et al., 2016; Clague et al., 2013; Nijman et al., 2005). Some DUBs display selectivity and specificity for particular ubiquitin linkages or cleaving positions within ubiquitin chains, whereas others show linkage ambiguity, mainly due to substrate selectivity via specific protein-protein interactions mediated through domains outside of the catalytic domain (Clague et al., 2019). The linkage specificities of human DUBs in the ubiquitin-specific protease (USP) and ovarian tumor (OTU) families have been systematically characterized *in vitro* (Faesen et al., 2011; Mevisen et al., 2013; Mevisen and Komander, 2017). Generally, the USP DUBs are not linkage but substrate specific (Faesen et al., 2011; Ritorto et al., 2014). By contrast, the OTU family DUBs display preference to diverse chains, unveiling the specificity rules of DUBs toward linkage (Mevisen et al., 2013). However, the Ub-linkage specificity *in vivo* is expected to be more complex and less explored because of DUBs' subcellular localization and PTMs, as well as the involvement of co-factors. DUBs are subjected to spacious and temporary regulation and can act as both negative and positive regulators in the ubiquitination system. Therefore, systematic analysis of the specificity of DUBs for ubiquitin linkages and substrates *in vivo* remains a challenge. Furthermore, for substrates with multiple ubiquitin chains, individual sites of ubiquitination may be modified by chains of different linkages and regulated by distinct DUBs. Therefore, it also remains challenging but deeply in demand to directly identify the modification sites on substrates, the ubiquitin chains, and corresponding enzymes involved in the modification process.

In this study, we combined yeast genetics and quantitative proteomics approaches to characterize the accumulation of seven lysine-linked ubiquitin chains in each DUB deletion strain, which might reflect the linkage specificity of DUBs *in vivo*. Utilizing the linkage specificity of certain DUBs, we developed a method termed DUB-mediated identification of linkage-specific ubiquitinated substrates (DILUS), which allowed us to build a network of specific protein substrates and their corresponding ubiquitinated lysine residues with certain ubiquitin linkages regulated by particular DUBs. After generating two large-scale datasets of the substrates and their ubiquitinated residues potentially modified with K63-linked chains for Ubp2, we further confirmed cyclophilin A (Cpr1) as an Ubp2 substrate that was modified with K63-linked chains at residue K151. These K63-linked ubiquitin chains could bind Zpr1 to trigger its nuclear translocation on the condition of glucose stimulus after starvation. However, the K48-linked chains at non-K151 sites of Cpr1 were mainly regulated by Ubp3 and mediated the degradation through proteasome.

## RESULTS

### Quantitative Proteomics Reveals Ubiquitin Chain Specificity of DUBs *In Vivo*

Although ubiquitin modifies thousands of proteins in yeast (Gao et al., 2016; Peng et al., 2003; Swaney et al., 2013), only 21 DUBs are known to be involved in deubiquitination. The budding yeast has five families of DUBs namely ubiquitin-specific proteases (USP, Ubp1–16), ubiquitin C-terminal hydrolases (UCH, Yuh1), ovarian tumor proteases (OTU, Otu1 and Otu2), JAB1/MPN/Mov34 metalloenzymes (JAMM, Rpn11) (Finley et al., 2012; Nijman et al., 2005), and a recently discovered MINDY protease (Miy1) (Abdul Rehman et al., 2016; Kristariyanto et al., 2017). As RPN11 (POH1 in human) is an essential gene in budding yeast (Finley, 2009), it is not included in this study.

First, we quantified the total ubiquitination level in WT and 20 DUB-deletion strains (Table S1) by performing western blotting and SILAC-based quantitative proteomics on total cell lysate (TCL) level (Figure S1). Both orthogonal methods showed different degrees of ubiquitinated protein accumulation in some DUB deletion strains such as *ubp3Δ*, *ubp7Δ*, and *ubp14Δ*, while being reduced in *ubp8Δ*, *ubp15Δ*, and *miy1Δ* strains (Figures S1B, S1C, and S1E). Next, the seven lysine-linked ubiquitin chains were globally compared in WT and DUB-deletion strains on the ubiquitin conjugates (UbC) level (Figure 1). The purified UbC was separated into three fractions based on molecular weight (<10, 10–50, and >50 kDa roughly representing mono ubiquitin, free ubiquitin chains, and ubiquitin conjugates, respectively) and then analyzed using a highly sensitive MS method called selective reaction monitoring (SRM) (Xu et al., 2009). In the <10 kDa section, the absence of some DUBs resulted in the accumulation of ubiquitin pool. However, the lack of proteasomal DUB Ubp6 led to a decrease of free ubiquitin, which was similar to a previous report (Nijman et al., 2005) (Figure S2A). In the 10–50 kDa section, UBP14 (USP5 in human) deletion resulted in a 30-fold increase in the abundance of K29- and K48-linked chains, but no significant changes in the abundance of K63-linked chains (Figure S2B). Our result is consistent with the previous reports that Ubp14 hydrolyzes unanchored ubiquitin chains (Amerik and Hochstrasser, 2004; Reyes-Turcu et al., 2009) and moreover indicates that the influence of Ubp14 on free chains is strongly linkage specific.

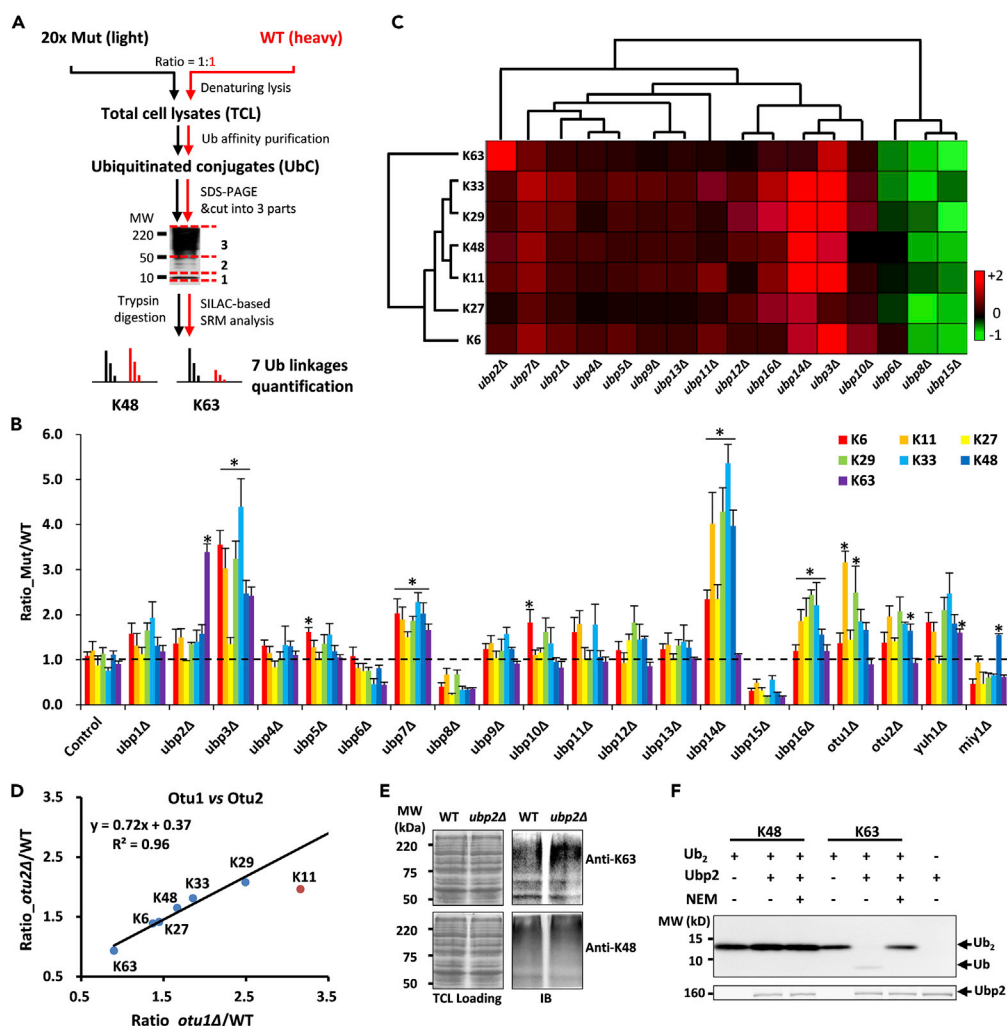


**Figure 1. Quantitative Proteomics of DUB-Deletion Strains Reveals Ubiquitin Linkage Specificity of Ubp2 for K63-Linked Chain**

(A) Schematic of SILAC-based quantitative proteomics used to quantify ubiquitin chains in DUB-deletion strains. Equal amounts of light- and heavy-isotope-labeled yeast of DUB-deletion and WT strains were mixed for LC-MS/MS analysis. Enriched ubiquitinated conjugates (UbC) under denatured conditions were separated into three fractions according to molecular weight (i.e., <10, 10–50 and >50 kDa). The seven ubiquitin chains were relatively quantified through selected reaction monitoring (SRM) technology.

(B) Ubiquitin chains in fraction 3 (MW > 50 kDa) were collected and measured by MS. Data were shown as mean  $\pm$  SEM of relative ratios for DUB-deletion and WT strains. Control and dotted line stand for quantification of equal light and heavy WT cells. The asterisk for significantly increased chains passed the *t*-test (*p*-value < 0.05).

(C) Hierarchical clustering analysis of seven ubiquitin chains quantification for each USP DUB-deletion strain (red, upregulation; green, downregulation; black, no change). The quantitative values were derived from panel (B).

(D) The seven chains accumulation comparison between OTU1- and OTU2-deletion strains.

(E) Ubp2 deletion resulted in the accumulation of K63- but not K48-linked chains. WT and *ubp2Δ* strains were harvested for immunoblotting with K63 (up) and K48 (down) chain-specific antibodies.

(F) Ubp2 specifically cleaves K63- but not K48-linked chains *in vitro*. The reaction was incubated at 37°C for 5 min before immunoblotting with monoclonal anti-ubiquitin antibody. Image was visualized by ECL.

See also Figures S1 and S2.

In the sector above 50 kDa, deletion of some DUBs (except Ubp6, Ubp8, Ubp15, and Miy1) resulted in significant accumulation of ubiquitination (Figure 1B). Most USP DUBs, such as Ubp1, Ubp7, and Ubp12, did not display obvious chain preferences. We also noticed that UBP3 deletion resulted in the accumulation of all of the chains except K27, whereas deletion of UBP2 specifically accumulated the K63 chain more than the

other six chains. As for the recently reported MINDY DUBs in yeast, deletion of MIY1 resulted in decreasing of overall ubiquitination level (Figure S1C), whereas the K48 chain levels obviously increased (Figure 1B).

In *S. cerevisiae*, only two open-reading frames encode OTU domain proteins (Otu1 and Otu2). Otu1 is orthologous to the human OTUD2 (38% identical in the OTU domain). It is reported through an *in vitro* assay that Otu1 and OTUD2 have similar biases toward atypical linkages, including K11, K27, K29, and K33 chains (Mevisse et al., 2013), while having a strong preference toward K11-linked chains. Interestingly, we found that OTU1 and OTU2 deletions caused similar accumulation patterns for six ubiquitin chains except K11-linked chains. The *otu1* $\Delta$  mutant accumulated more K11-linked chains than the *otu2* $\Delta$  strain (Figure 1D). Despite possible side effects of DUBs deletions *in vivo*, the observed specificities of DUBs toward ubiquitin linkages were consistent between *in vivo* and *in vitro* studies.

### Ubp2 Preferentially Regulates K63-Linked Chains

Ubp2 is reported to preferentially bind K63- over K48-linked chains and antagonize Rsp5-mediated assembly of K63-linked chains (Kee et al., 2005, 2006). Our analysis also proved that UBP2 deletion selectively increased the abundance of K63-linked chains compared with the other chains (Figures 1B and 1C). Additionally, across the 20 DUB-deletion strains, the abundance of K63-linked chains was presented as the highest accumulation in the *ubp2* $\Delta$  strain. We further confirmed this preference accumulation of the K63-linked instead of K48-linked chains in *ubp2* $\Delta$  by linkage specific antibodies on TCL (Figure 1E). Furthermore, we characterized Ubp2 activity by performing *in vitro* deubiquitination assays. The result showed that Ubp2 cleaved K63-linked chains with high activity while having little effect on K48-linked chains (Figure 1F). These pieces of evidence indicated that Ubp2 specifically participated in the regulation of substrates, which modified with K63-linked chains in yeast.

### Ubp2 Substrate Profiling by DILUS Strategy

To fully characterize the regulatory mechanism of a given DUB or E3, it is often necessary to screen its regulated substrates and further distinguish their relevant ubiquitination sites. The classical proteomic strategy to systematically screen the substrates of these UPS enzymes is comparing the difference of the ubiquitinated conjugates before and after that enzyme overexpression or knockout (Raman et al., 2015; Silva et al., 2015; Xu et al., 2009; Zhuang et al., 2013). However, the ubiquitination heterogeneity shows that multiple lysine residues of the substrate are modified with diverse chains. Therefore, in addition to upregulated UbC levels (Figure 2A, class I), upregulated modified sites without changes in UbC levels (Figure 2A, class II, *k1* site) in the *ubp2* $\Delta$  strain are also potential substrates of Ubp2. Combined with the specificity and ubiquitination heterogeneity, we developed a differential display strategy termed DILUS aimed at identifying Ubp2-regulated substrates and modification sites. Because the Ubp2 deletion specifically accumulated the K63-linked chain, upregulated sites were potentially modified with K63-linked chains with high possibility. In addition, we quantified the proteome of the *ubp2* $\Delta$  and WT through SILAC and eliminated the false-positive targets that were also increased on TCL levels (Table S2).

We compared UbC and K- $\epsilon$ -GG peptides between *ubp2* $\Delta$  and WT using an SILAC label-swap strategy. The UbC samples were enriched with Ni-NTA agarose and the modified peptides with a K- $\epsilon$ -GG antibody (Figure S3A). For UbC enrichment, high-quality ubiquitinated samples were purified under denaturing conditions (Figure S3B), and three separation strategies were applied to improve coverage of UbC and their K- $\epsilon$ -GG modified sites (Figures S3C–S3E). In the UbC and K- $\epsilon$ -GG antibody-enriched experiments, we totally quantified 2,990 and 965 ubiquitinated proteins, with 579 and 2,091 K- $\epsilon$ -GG peptides, respectively (Figure 2B and Table S4). We noted that there was a small overlap of modified peptides identified from these two enrichment datasets (Figure 2C), indicating the complementary effects of the two methods for the identification of the ubiquitination events.

In the UbC dataset, 22 upregulated ubiquitinated proteins without change on the TCL were outlined in the *ubp2* $\Delta$  strain (Figure 3A and Table S3). Unexpectedly, the known Ubp2 substrates, such as 40S ribosomal protein S3 (Rps3) and EH domain-containing and endocytosis protein 1 (Ede1) (Silva et al., 2015; Sims et al., 2009), were not accumulated significantly on the UbC quantification (Figure 3A). Through DILUS strategy, the upregulated K- $\epsilon$ -GG peptides were also considered as potentially modified sites regulated by Ubp2 (Figure 3B). In the UbC dataset, 36 upregulated K- $\epsilon$ -GG peptides, including Rps3 (K212) and Ede1 (K1329), were significantly increased in the *ubp2* $\Delta$  strain, which proved that the DILUS strategy could identify the true substrates missed by the classical method. To amplify the power of DILUS, the combination

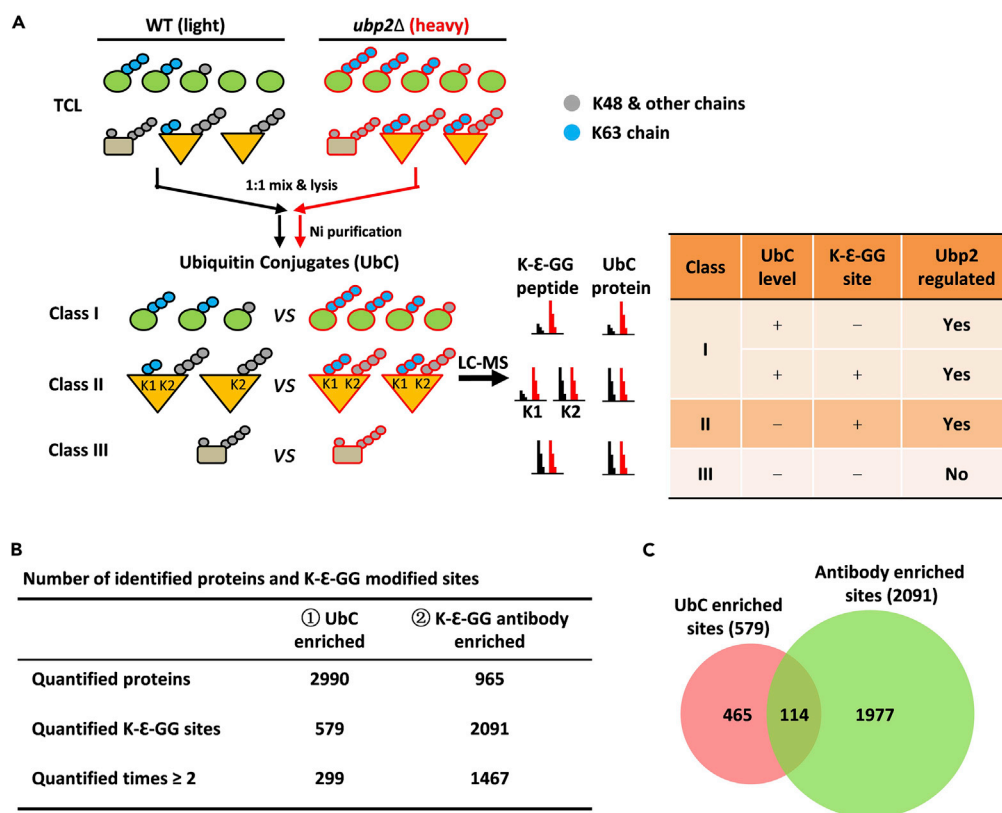


**Figure 2. DUB-Mediated Identification of Linkage-Specific Ubiquitinated Substrates (DILUS) Requires Deep Coverage of the K- $\epsilon$ -GG-Modified Sites**

(A) Schematic diagram of DILUS strategy used to directly screen for Ubp2-regulated substrates and sites potentially modified with K63-linked chains. All of the ubiquitin conjugates were divided into three classes and only classes I and II are true targets of Ubp2. After trypsin digestion, ubiquitin modified substrates will produce ubiquitin-remnant-containing (K- $\epsilon$ -GG) peptides. In class I, Ubp2 deletion resulted in increased levels of UbC with or without increased K- $\epsilon$ -GG peptides identified. In class II, only the level of K- $\epsilon$ -GG peptides (modified site lysine K1) impacted by Ubp2 would increase, whereas other K- $\epsilon$ -GG-modified peptides (modified site lysine K2) will be not affected by UBP2 deletion. “+” stands for “increased in *ubp2Δ* strain” and “-” for “no change or not identified in *ubp2Δ* strain”.

(B) Comparison of identified K- $\epsilon$ -GG peptides from the UbC and K-GG enrichment experiments.

(C) The overlap of K- $\epsilon$ -GG-modified site identified from UbC and K- $\epsilon$ -GG antibody enriched methods.

See also Figure S3.

with K- $\epsilon$ -GG antibody enrichment allowed 228 upregulated peptides to be filtered out (Figure 3C) and 20 of them overlapped with the upregulated peptides obtained from the UbC dataset (Figure 3D). These results showed that each protein contained only certain upregulated K- $\epsilon$ -GG modified sites (Table S4), suggesting that Ubp2 specifically regulated only a subset of sites within these substrates. The number of substrate candidates from class II was much larger than that from class I (Figure 3E). Ultimately, we combined the potential substrates derived from UbC and K- $\epsilon$ -GG site datasets and identified 166 proteins with 244 sites that were potentially modified with K63-linked chains and regulated by Ubp2 (Table S5). Gene ontology (GO) classification analysis revealed that Ubp2 substrates potentially modified with K63-linked chains participated in a broad range of cellular processes (Figure 3F and Table S6), including endocytosis, amino acids transmembrane transport, and protein translation.

### The Ubiquitination at K151 Site of Cpr1 Is Regulated by Ubp2

We noticed that most potential substrate candidates identified by DILUS were not changed on the TCL and UbC level in the *ubp2Δ* strain. These substrates were regulated by Ubp2 on certain but not all sites and potentially modified with K63-linked chains, which belonged to class II (Figure 2A). To confirm the effect of DILUS strategy, we chose one novel substrate potentially regulated by Ubp2 for further analysis. The

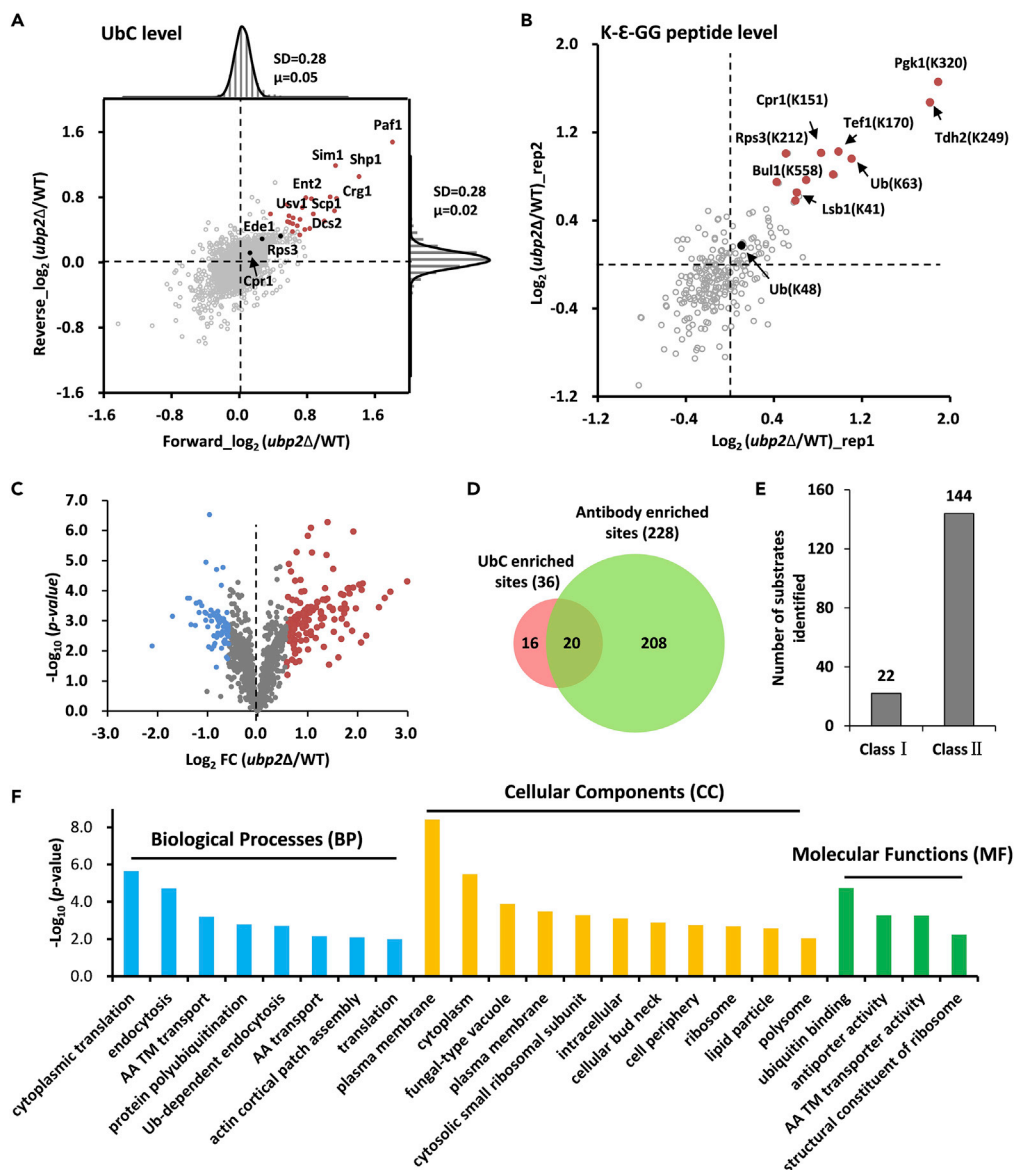


**Figure 3. Identification of Ubp2's Substrates Potentially Modified with K63-Linked Chains through DILUS Approach**

(A) Global distribution of ubiquitinated proteins in label-swapped samples. The top and right shows the distribution of log<sub>2</sub> ratios of quantified proteins in the forward (*ubp2Δ*/WT, *n* = 2,689) and reverse (*ubp2Δ*/WT, *n* = 2,777) experiments. Proteins quantified in both experiments (*n* = 2,475) were shown in the central scatterplot. The red dots stand for potential substrates of Ubp2 derived from UbC level quantification.

(B) Global distribution of K-ε-GG peptides in label-swapped UbC samples. K-ε-GG peptides with only one quantification value were not shown. The red dots stand for potential sites regulated by Ubp2 derived from UbC-enriched dataset.

(C) Volcano plot of log<sub>2</sub> fold change (FC, *ubp2Δ*/WT) against -log<sub>10</sub> *p*-value from the *t*-test. The red dots were for potential sites regulated by Ubp2 derived from K-ε-GG-antibody-enriched dataset.

(D) The overlap of increased modified sites from UbC-enriched and K-ε-GG-antibody-enriched methods.

(E) The number of identified substrates modified with K63-linked chains as determined based on increased UbC level (class I) or K-ε-GG-modified site level (class II). The false-positive targets increased on TCL were filtered out.

(F) GO analysis of the substrates regulated by Ubp2 and potentially modified with K63-linked ubiquitin chain. AA stands for amino acid and TM for transmembrane.

See also Tables S3, S4, S5, and S6.

cyclophilin (Cpr1) from the UbC dataset was not altered after UBP2 deletion (Figure 3A), but the K151-modified site was increased (Figure 3B).

It is well known that cyclosporin A (CsA) inhibits T cells by blocking signal transduction (Breuder et al., 1994; Zhu et al., 2015), and Cpr1 is a target of CsA. This study as well as previous reports have shown that Cpr1 is highly ubiquitinated (Swaney et al., 2013), but the biological function of these ubiquitination events, as well as the linkage types and its regulating DUBs, are unknown. First, we expressed and purified the histidine and biotin (HB)-tagged Ubp2 and its blank control for LC-MS/MS analysis. Ubp2 was significantly enriched compared with the vector control, and the Cpr1 was also enriched significantly (Figure 4A), thus Ubp2 could interact with Cpr1. Then, we tagged Cpr1 with same histidine and biotin tags and expressed it in WT and *ubp2Δ* strains. We compared their ubiquitinated forms after enrichment; the western blotting suggested that ubiquitinated Cpr1, especially those of higher molecular weight, were more abundant in *ubp2Δ* than in WT (Figure 4B), suggesting that Cpr1 ubiquitination was affected by Ubp2. SILAC-based quantitative proteomics revealed that Cpr1 has at least seven lysine residues modified with ubiquitin (Figure 4C). However, K-ε-GG peptide at Cpr1-K151 was elevated in the *ubp2Δ* to a greater extent than those peptides corresponding to other sites, indicating that Ubp2 specifically regulated the ubiquitination at K151 in preference to other sites (Figure 4C, up). In addition, the level of unmodified peptides at Cpr1-K151 was significantly less than that of other peptides (Figure 4C, down) as a result of a greater proportion of modified K151 sites, because of the total amount of Cpr1 in the *ubp2Δ* strain being unaltered.

After tandem affinity purification (TAP) in denatured condition, Cpr1 and ubiquitin were the most abundant, and contaminants were reduced effectively (Figure 4D). The K48-linked chain on Cpr1 was not obviously increased in the *ubp2Δ* strain, whereas the K63-linked chain was increased up to four times compared with WT (Figure 4E). The accumulation of K63-linked chain on Cpr1 was Ubp2 catalytic activity dependent; because this increase could not recover even we re-expressed a catalytic inactive mutant Ubp2-C745S in *ubp2Δ* strain (Figure 4F). Conclusively, Ubp2 participated in the regulation of ubiquitination at K151 site of Cpr1.

### The K151 Site of Cpr1 Is Modified with K63-Linked Ubiquitin Chain

To further prove that K63-linked chains was modified at the Cpr1 K151 site, we constructed strains expressing either CPR1 or *Cpr1-K151R* mutant tandemly tagged with 6×histidine and biotin on their C-termini—hereafter referred to Cpr1-WT and *Cpr1-K151R* mutant (Figure 5A). To improve accuracy, we tandemly purified and quantified Cpr1 and *Cpr1-K151R* through SILAC label-swap strategy (Figure S4A). First, we confirmed the effects of the *Cpr1-K151R* mutation on Cpr1 abundance. We chose three peptides allowing quantification of wild-type Cpr1, namely, (Pep\_1: VESLGSPSGATK), *Cpr1-K151R* (Pep\_2: VESLGSPSGATR), and shared peptide of Cpr1 and its mutant (Pep\_3: GFGYAGSPFHR; Figure S4B). The abundance of Cpr1 did not change in the *Cpr1-K151R* mutant (Figures 5B and S4C), suggesting that ubiquitin chain modification at Cpr1-K151 had no effect on its abundance. After TAP, the MS analysis showed that Cpr1 and ubiquitin were the most abundant, and contaminants were reduced effectively (Figure 5C). The Cpr1 contained large amounts of K48- and K63-linked chains but only a small amount of K11-linked chains (Figure 5D). Surprisingly, we found that the amount of K63-linked chains in WT was 10-fold higher than in *cpr1-K151R* mutant (Figures 5E and S4D). However, no significant difference was detected in the abundance of K48-linked chains (Figures 5E and S4E). These results strongly indicated that Cpr1 was modified with K48- and K63-linked ubiquitin chains and that Ubp2 recognized and cleaved K63-linked chains at K151 but not K48-linked chains at other sites.

### The K63-Linked Chain at K151 Site of Cpr1 Mediates the Nuclear Translocation of Zpr1

To investigate the biological function of the K63-linked chains at the Cpr1 K151 site, we employed an SILAC-based TAP strategy to profile the Cpr1 interactome (Figures 6A and S5A) and the putative interacting proteins of K63-linked chains at the Cpr1 K151 site (Figures 6B and S5B). After TAP in native conditions, the abundance of Cpr1 and *Cpr1-K151R* in SDS-PAGE resolved samples was measured through silver staining (Figure S5C). Figure 6A showed the upregulated proteins that interacted with Cpr1 (Table S7), including positive controls such as Ess1 (Ansari et al., 2002). We noticed that Rsp5, an E3 ligase of NEDD4 family that catalyzes the synthesis of K63-linked ubiquitin chains, was also enriched. Additionally, we identified those interacting proteins that were decreased when Cpr1 was mutant at the K151 site (downregulated proteins in the third quadrant in Figure 6B and Table S7). Interestingly, a majority of these interacting proteins were overlapped with the Cpr1 interactome (Figure 6C). Gene ontology classification of these interacting

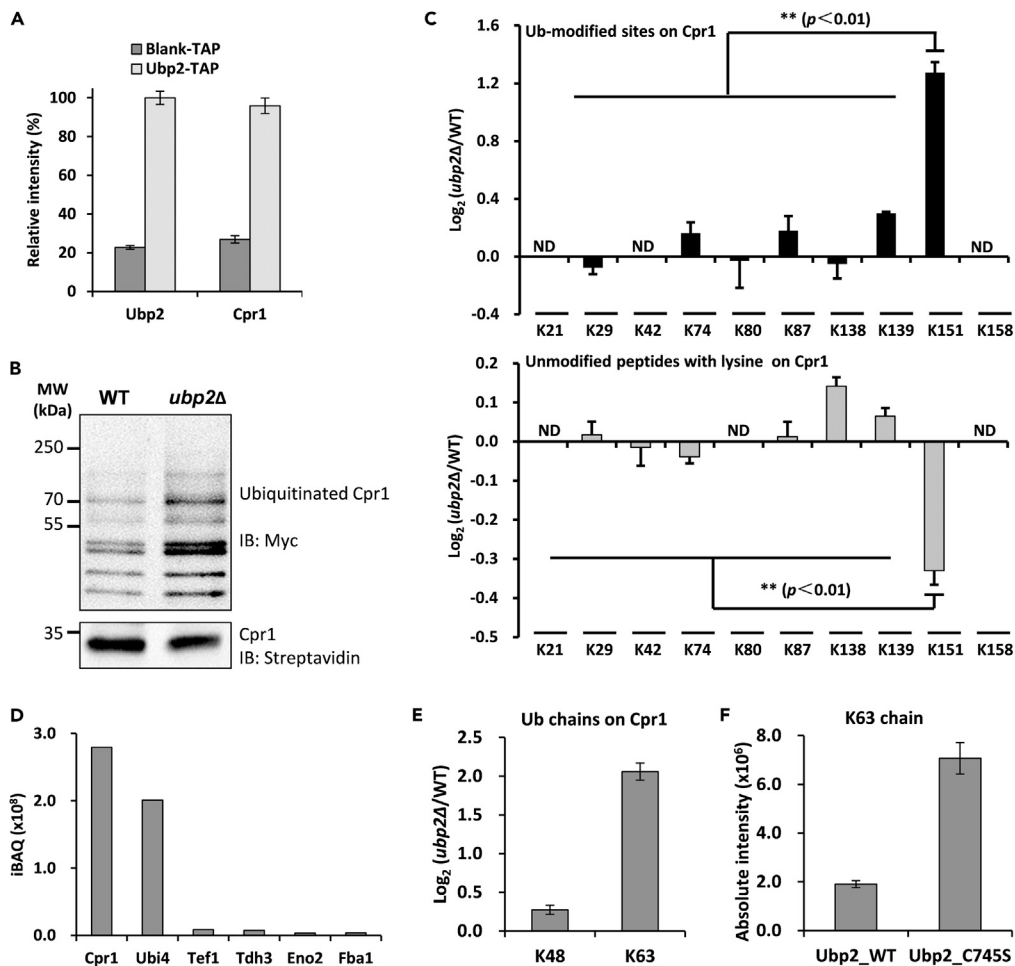


#### Figure 4. The Ubiquitination at K151 Site of Cpr1 Is Regulated by Ubp2

(A) Ubp2 interacted with Cpr1. Label-free quantification of the bait protein Ubp2 in the yeast expressing HB tag vehicle (Blank) and HB-tagged Ubp2 (HB-Ubp2) after TAP. Equal amounts of yeast cells were used, and the purifications were operated in parallel.

(B) Western blotting for Cpr1 in WT and *ubp2Δ* strains. WT and *ubp2Δ* strains expressing HB-tagged Cpr1 were subjected to TAP and immunoblotting Cpr1 and its ubiquitinated forms with anti-streptavidin and anti-Myc antibodies based on the biotin tag on Cpr1 and the myc tag on Ub, respectively.

(C) Log<sub>2</sub> ratios of K-ε-GG peptides (up) and unmodified peptides with lysine on C-terminal (down) after tryptic-cleaved Cpr1 in WT and *ubp2Δ*. The error bars represent mean ± SEM from two biological replicates quantifications. The asterisk (\*\*) indicated the *p*-value < 0.01 using *t*-test. ND was for no detection.

(D) The top six proteins identified in tandemly purified Cpr1 with HB tag under denatured condition.

(E) The K63 but not K48 chains on Cpr1 increased in the *ubp2Δ* strain. Data shown as mean ± SEM from two biological replicates quantifications.

(F) The K63 chain on Cpr1 was regulated by Ubp2 depending on USP catalytic activity. The K63-linked ubiquitin chain on Cpr1 was increased in the Ubp2 C745S mutant strain. The results were normalized with the amount of unmodified Cpr1 and shown as mean ± SEM.

proteins revealed that the K151R substitution perturbs the Cpr1 interactome in a profound manner during the starvation, amino acid metabolism, and endocytosis processes. These results indicated that K63-linked chains at Cpr1-K151 executed some cellular functions (Figure 6D).

Among the K151-dependent Cpr1-interacting proteins, Zpr1 (zinc finger protein) decreased its association with the *Cpr1-K151R* mutation. Previous studies have shown that Zpr1 interacts with ubiquitin and undergoes nuclear translocation following mitogen treatment (Ansari et al., 2002). Structure analysis showed that Zpr1 owned two zinc finger domains, which might interact with the K63-linked chain. We incubated

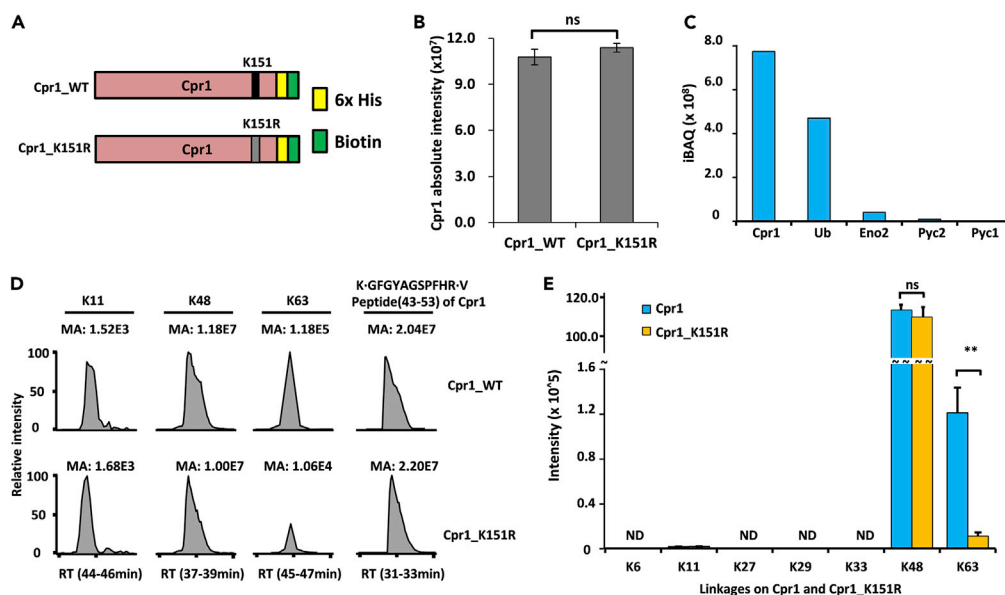


**Figure 5. The K151 Site of Cpr1 Is Modified with K63-Linked Chain**

(A) Schematic for the construction of HB tagged Cpr1 and its K151R mutant.

(B) The Cpr1 amount was not affected in the K151R mutant. Data shown as mean  $\pm$  SEM from two biological replicates quantifications.

(C) The identified proteins from tandemly purified Cpr1 with HB tag under denatured conditions.

(D) HPLC chromatographic peaks of the identified Ub chains on Cpr1 and Cpr1-K151R. The peak area (AA) corresponds to the relative ion intensity of the target peptide. Three Ub-linkages (K11, K48, and K63) were detected. One of tryptic peptide (GFGYAGSPFHR) shared by Cpr1 and Cpr1-K151R was used as quantitation control.

(E) Swapped SILAC-based quantitative proteomics of tandemly purified ubiquitin chains for WT and Cpr1-K151R mutant. Light- and heavy-isotope-labeled amino acids were incorporated into Cpr1 and Cpr1-K151R in cell culture. Yeast cells were lysed under denatured conditions and then tandemly purified with HB tags. The error bars were represented mean  $\pm$  SEM from two biological replicates quantifications.

See also Figure S4.

recombinant Zpr1 with equal amounts of K48- and K63-linked ubiquitin chains ( $N = 2-7$ ) and then washed with PBS thoroughly for far-western blotting analysis (Xiao et al., 2020). We found that its interaction with K63-linked chains was stronger than K48-linked chains (Figure S6A). Furthermore, Zpr1 displayed higher affinity for longer over shorter K63-linked chains (Figure S6B).

Previous studies show that Zpr1 is in the nucleus of growing cells and relocates to the cytoplasm during starved status via a Cpr1-mediated process (Ansari et al., 2002). In this study, yeast cells expressing Zpr1-GFP and Cpr1-mcherry were grown to log phase in a rich YEPD medium and starved in a glucose-free synthetic complete medium overnight and then retreated with glucose. Zpr1 was found in the cytoplasm after 12 h of nutrient withdrawal (upper left panel of Figures 6E and 6F); it was almost entirely translocated to the nucleus following the addition of glucose (left lower panel of Figure 6E and upper right panel of Figure 6F). Cpr1 was co-localized with Zpr1 in the cytoplasm under starvation and then translocated to the nucleus in the presence of glucose (Figures 6E and S7). In contrast, glucose treatment did not activate Zpr1 translocation in the starved *cpr1* $\Delta$  strain, suggesting the importance of Cpr1 in this process. Interestingly, the Cpr1-K151R substitution of Cpr1 reduced the efficiency of translocation to less than half, and similar effects were also observed in the ubiquitin K63R mutant. On the contrary, Ubp2-C745S mutant accelerated the Zpr1 nuclear translocation in some degree (Figures 6F and 6G). These results collectively suggested that the K63-linked chain at Cpr1-K151 and its regulation by Ubp2 were critical for Zpr1 translocation.

### Ubp3-Mediated Cleavage of K48-Linked Chains at Non-K151 Sites of Cpr1 Triggers Proteasomal Degradation

As not all of the ubiquitination sites were regulated by Ubp2, we speculated that there exist other DUBs regulating the ubiquitination especially for the K48-linked chains on the Cpr1. To identify DUBs involved

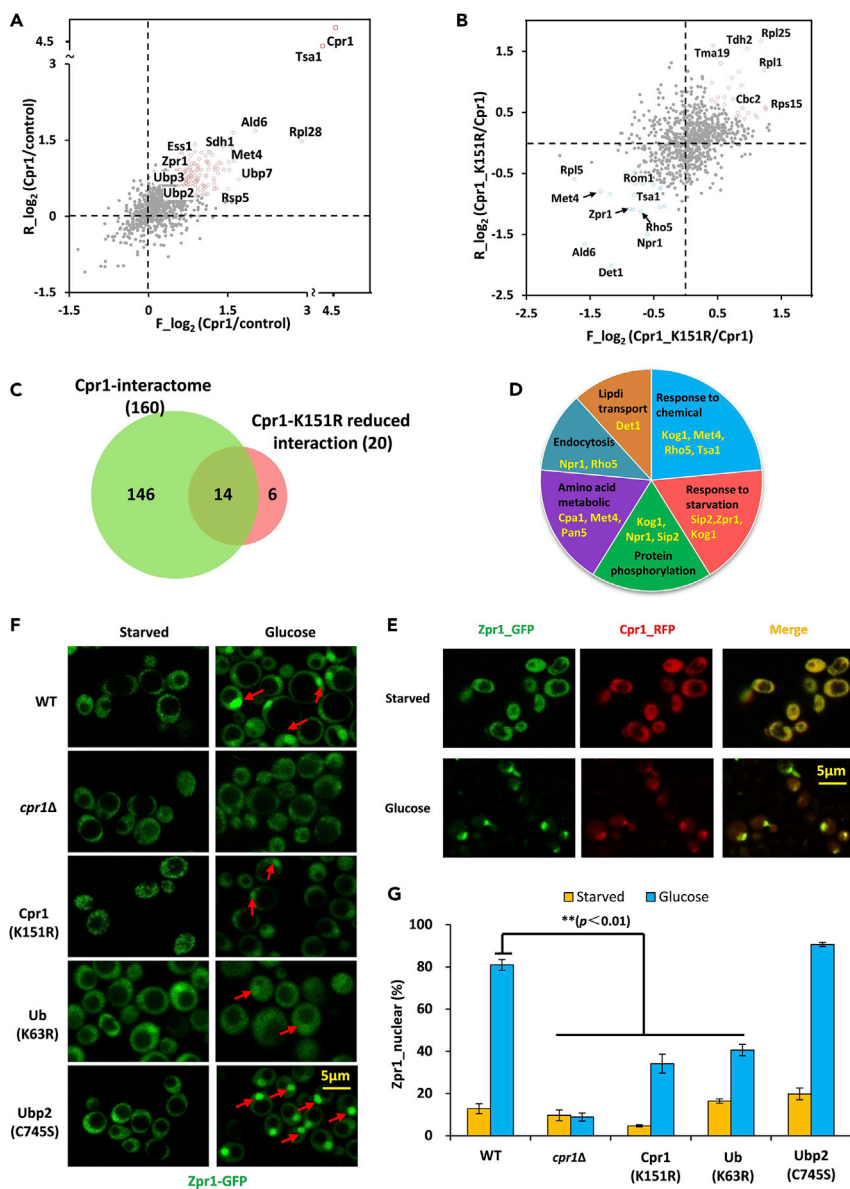


**Figure 6. The K63-Linked Chain at K151 Site of Cpr1 Promotes Nuclear Translocation of Zpr1**

(A) Global distribution of Cpr1-interacting proteins (shown in red) in SILAC label-swapped samples.

(B) Global distribution of all Cpr1- and its K151R mutant-interacting proteins. The blue points represented interacting proteins specific for K63-linked chains at K151 of Cpr1.

(C) Overlap between Cpr1-interacting proteins (left) and proteins that interacted with K63-linked chains at K151 of Cpr1 (right).

(D) Gene ontology classification for proteins that interacted with K63-linked chains at K151 of Cpr1.

(E) Both Zpr1 (green) and Cpr1 (red) moved from cytoplasm to the nucleus following glucose treatment. Areas of colocalization were shown in yellow (merged images, scale bar = 5  $\mu$ m).

(F) The nuclear transport of Zpr1 following glucose treatment was reduced in *Cpr1-K151R* mutants and blocked in the Cpr1-deletion strain. WT, *cpr1* $\Delta$ , *Cpr1-K151R*, *ubiquitin-K63R*, and *Ubp2 C745S* mutants expressing Zpr1-GFP were grown to log phase in YEPD medium, starved in glucose-free synthetic complete medium for 12 h, and then treated with glucose (scale bar = 5  $\mu$ m).

(G) Percentage of Zpr1 that was transported to the nucleus prior to and after glucose treatment. Data were shown as mean  $\pm$  SEM obtained from three independent experiments ( $\sim$ 100 yeast cells per experiment).

See also [Figures S5–S7](#) and [Table S7](#).

in the regulation of non-K63-linked chains on Cpr1, we reanalyzed the Cpr1 interactome dataset and found that besides Ubp2, Ubp3 and Ubp7 were also found to be Cpr1-interacting proteins (Figure 6A). The Ubp3-Cpr1 interaction was in agreement with a previous report (Ossareh-Nazari et al., 2010). To further validate the interaction, we constructed HB-tagged Ubp3 and proved that Cpr1 was found to interact with Ubp3 (Figure 7A). Because Ubp7 did not significantly affect the ubiquitination of Cpr1 (data not shown), Ubp7 was not included for further analysis in this study.

We further investigated the role of Ubp3 in the deubiquitinating regulation of Cpr1. The western blotting results suggested that ubiquitinated Cpr1, especially those of higher molecular weight, were much more abundant in *ubp3Δ* than in WT (Figure 7B). This indicated that Cpr1 ubiquitination was significantly affected by Ubp3. SILAC-based quantitative proteomics showed that the lack of Ubp3 increased the K-ε-GG peptides of Cpr1 at all sites including the K151 site (Figure 7C). The K48- and K63-linked chains on Cpr1 were both significantly increased (Figure 7D). Figure 1B showed that Ubp3 was chain-unspecific and the second most important DUB regulating K63-linked chains in yeast. Furthermore, we characterized Ubp3 activity by performing *in vitro* deubiquitination assays. Ubp3 cleaved both K48- and K63-linked chains with high activity (Figure 7E). These results indicated that Ubp3 also regulated K63-linked chains at K151 and K48-linked chains at non-K151 sites of Cpr1.

We further investigated the biological effects of K48-linked chains on Cpr1. Following the treatment with a proteasome inhibitor MG132, the abundance of both K48-linked chains and Cpr1 increased with time of incubation (Figure 7F). LC-MS/MS results also showed that the amount of Cpr1 in TCL increased about two-fold after MG132 treatment (Figure 7G), consistent with western blot results, suggesting that the degradation of Cpr1 was mediated by the proteasome. The abundance of K48-linked chains on Cpr1 increased more than two-fold, whereas the abundance of K63-linked chains remained stable after MG132 treatment (Figure 7H), suggesting that K48-linked chains regulate the Cpr1 level through proteasomal degradation. The abundance of non-K151 K-ε-GG peptides was significantly increased after MG132 treatment but that of K151 was not impacted by MG132, further implying the different functions of these ubiquitin chain types (Figure 7I).

## DISCUSSION

There are eight types of ubiquitin chains, whereas we focus on seven lysine-linked ubiquitin chains and exclude linear chain in this study. This is because the N-terminal tags on ubiquitin are introduced in WT (JMP024) strain.

Previous *in vitro* deubiquitinating assays provide pivotal and efficient evidences for the activity and specificity of DUBs to pure ubiquitin chains (Mevisse et al., 2013; Ritorto et al., 2014). Four mechanisms underlying the linkage specificity of the OTU class of DUBs have been concluded (Mevisse et al., 2013). However, the linkage specificity of DUBs *in vivo* is more complex and poorly understood. In cells, DUBs are tightly regulated in space and time and can act as negative or positive regulators of the ubiquitin system including E2 and E3, which may be direct or indirect regulation of the ubiquitin chains. For example, the human OTUB1 is specific for cleaving K48-linked ubiquitin chains and has no activity for K63-linked chains in an *in vitro* assay. However, both K48- and K63-linked chains were accumulated in OTUB1 deletion cells. Further analysis reveals that OTUB1 binds to the E2 UBC13 *in vivo*, which inhibits the extension of the K63-linked chain (Juang et al., 2012).

To determine the linkage specificity of DUBs *in vivo*, we assumed that a specific DUB deletion would result in the accumulation of its preferred linkages. Although this accumulation may be a result of direct or indirect effects because of the loss of certain DUB, the results provide us some valuable hints reflecting the specificity of DUBs to ubiquitin chains. For the USP family, most of them were not linkage specific, whereas the specificity of Ubp2 toward K63-linked chains was verified through *in vitro* and *in vivo* assays. Ubp14 was preferred to all six free ubiquitin chains except K63-linked forms *in vivo*. Here, we also confirmed that Otu1 could specifically regulate more K11-linked chains modified on substrates than Otu2 *in vivo*, which was consistent with those from *in vitro* assay studies (Mevisse et al., 2013). Conclusively, we noted that *in vivo* assays may not always be straightforward to interpret because of competing effects of other DUBs in the cell. Therefore, *in vivo* and *in vitro* assays are best used in combination for studying the specificity of DUBs.



quantification of K- $\epsilon$ -GG peptides, allowing us to identify site-specific modifications of certain ubiquitin linkage on substrates regulated by Ubp2 (Figure 2A). For DILUS approach, however, it required that Ubp2 or any other chain-specific DUB of choice to obviously increase the specific chain but not the mono-ubiquitination (Kee et al., 2006). If not, it was hard to speculate the chain types bound on the substrates through the MS quantitative analysis. The further combination of DILUS with the K- $\epsilon$ -GG antibody enrichment strategy enabled more site-specific identification with certain linkages (Kim et al., 2011; Tong et al., 2014; Udeshi et al., 2013). With more modification sites being systematically identified and quantified in Ubp2 and other DUBs, robust evidence and a stronger conclusion about the determining elements for the substrate specificity of DUBs can be obtained in the future.

Different sites of Cpr1 are modified by different ubiquitin chain types. However, it is unclear how DUBs specifically distinguish and regulate these ubiquitin chains and what roles these modifications played before. What determines the regulation and how the DUBs cooperate with each other for substrate ubiquitination will require more research. The K63-linked chains at K151 of Cpr1 mediated interaction with Zpr1. The zinc finger domain of Zpr1 may interact with a K63-linked chain with higher affinity than a K48-linked chain. Additionally, the affinity capacity of the Zpr1 with K63-linked chain was increased with the length of the chain (Figure S6). In future studies, more evidence should be added to support this potential new ubiquitin-binding domain for K63-linked chains. The absence of K63-linked chains in Cpr1-K151R mutant significantly hindered the interaction between Cpr1 and Zpr1, thereby impacting the translocation of Zpr1 from cytoplasm to the nucleus in starved cells following glucose treatment. We also found that the K151R mutation reduced but did not block Zpr1 nuclear translocation because the process was rescued by the extension of glucose stimulation (data not shown). The results suggest that other mechanisms might exist to regulate the translocation of Zpr1 from cytoplasm to nucleus, including the compensatory mechanism of K63-linked chain on other sites of Cpr1. The molecular mechanisms underlying this process require further study.

In conclusion, the results of DUBs for ubiquitin chains bearing different linkages reflected the *in vivo* specificity. Using the linkage and site specificities, we developed a novel strategy, DILUS, to determine the sites on substrates favorable to decoding the ubiquitin code. Using this strategy, we identified substrates of Ubp2 modified by K63-linked chains and provided the detailed mechanism of how DUBs edit and regulate ubiquitination precisely. The balance of different chains on certain sites of Cpr1 regulated by specific DUBs is tightly coupled to the regulation of protein levels and signaling functions. These findings not only provide new insights into the regulatory mechanisms underlying deubiquitination but also reveal complicated ubiquitination networks, transduction pathways, and biological functions.

### Limitations of the Study

Although we aimed to reflect the ubiquitin chain specificity of DUBs *in vivo*, we could not exclude the side effects of DUBs deletion. For example, certain DUB might affect the ubiquitin transcription and the stability of E2 or E3, which made it more complex for specificity research *in vivo*. We thus recommended to verifying their linkage specificity additionally with *in vitro* assays. Second, although Ubp2 preferred to cleave the K63 linkage, we still could not completely exclude the substrate candidates modified with mono-ubiquitination or other chains potentially affected by Ubp2 when using DILUS strategy. For this limitation, we could use the tools of K63-UIM (ubiquitin interacting motif) (Sims and Cohen, 2009) to reduce the interference. K63-UIM could specifically interact with K63 ubiquitin chains with high affinity than other chains and mono ubiquitin, thus combined K63-UIM enrichment with DILUS strategy would be a perfect method to screen the specific substrates of Ubp2. Finally, despite we had screened a series of potential candidate substrates of Ubp2 through DILUS strategy, additional molecular and biochemical validations would be recommended to verify the target substrates.

### METHODS

All methods can be found in the accompanying [Transparent Methods supplemental file](#).

### DATA AND CODE AVAILABILITY

The mass spectrometry proteomics data have been deposited to the ProteomeXchange Consortium (<http://proteomecentral.proteomexchange.org>) via the iProX partner repository (Ma et al., 2019). The

accession numbers for the mass spectrometry proteomics data reported in this paper are the ProteomeXchange dataset identifier: PXD017357 and the iProX (<https://www.iprox.org/>) dataset identifier: IPX0001986000.

## SUPPLEMENTAL INFORMATION

Supplemental Information can be found online at <https://doi.org/10.1016/j.isci.2020.100984>.

## ACKNOWLEDGMENTS

We are grateful to Drs. Wei Xiao, Junmin Peng, Felix Cheung, Anthony Nguyen, Miguel Prado, and Eric Dammer for critical review of the manuscript. We thank Drs. Joseph Heitman, Lilin Du, Donald Kirkpatrick, and Yanchang Wang for gracious gifts of their reagents, strains, and ubiquitin linkage-specific antibodies. We are indebted to Drs. Jingwei Wang, Tianying Yu, Limei Zhou, and Chen Deng for support in the early stage of this project. This study was supported by the Chinese National Basic Research Programs (2017YFA0505100, 2017YFA0505002, 2017YFC0906600, & 2017YFC0906700), the National Natural Science Foundation of China (31700723, 31670834, 31870824, 31901037, & 91839302), the Innovation Foundation of Medicine (16CXZ027, AWS17J008, & BWS17J032), National Megaprojects for Key Infectious Diseases (2018ZX10302302), Guangzhou Science and Technology Innovation & Development Project (201802020016), the Unilevel 21st Century Toxicity Program (MA-2018-02170N), the Foundation of State Key Lab of Proteomics (SKLP-K201704), and the National Institutes of Health of United States grant (R37GM43601) to D.F.

## AUTHOR CONTRIBUTIONS

P.X. and Y.L. designed experiments. Y.L. and Q.L. performed most of the experiments with the help of Y.G. and Z.X.. Y.L. and Q.L. collected and analyzed all the data with the help of Y.W., C.X., Q.L., and L.C. constructed all the DUB's knockout strains. Y.L. and P.X. wrote the manuscript with input from all authors. J.W., Z.D., F.H., and D.F. offered advice and discussion for the manuscript.

## DECLARATION OF INTERESTS

The authors declare no competing interests.

Received: June 14, 2019

Revised: January 16, 2020

Accepted: March 9, 2020

Published: April 24, 2020

## REFERENCES

- Abdul Rehman, S.A., Kristariyanto, Y.A., Choi, S.Y., Nkosi, P.J., Weidlich, S., Labib, K., Hofmann, K., and Kulathu, Y. (2016). MINDY-1 is a member of an evolutionarily conserved and structurally distinct new family of deubiquitinating enzymes. *Mol. Cell* 63, 146–155.
- Amerik, A.Y., and Hochstrasser, M. (2004). Mechanism and function of deubiquitinating enzymes. *Biochim. Biophys. Acta* 1695, 189–207.
- Ansari, H., Greco, G., and Luban, J. (2002). Cyclophilin A peptidyl-prolyl isomerase activity promotes ZPR1 nuclear export. *Mol. Cell Biol.* 22, 6993–7003.
- Breuder, T., Hemenway, C.S., Movva, N.R., Cardenas, M.E., and Heitman, J. (1994). Calcineurin is essential in cyclosporin A- and FK506-sensitive yeast strains. *Proc. Natl. Acad. Sci. U S A* 91, 5372–5376.
- Chen, D., Liu, X., Xia, T., Tekcham, D.S., Wang, W., Chen, H., Li, T., Lu, C., Ning, Z., Liu, X., et al. (2019). A multidimensional characterization of E3 ubiquitin ligase and substrate interaction network. *iScience* 16, 177–191.
- Clague, M.J., Barsukov, I., Coulson, J.M., Liu, H., Rigden, D.J., and Urbe, S. (2013). Deubiquitylases from genes to organism. *Physiol. Rev.* 93, 1289–1315.
- Clague, M.J., Urbe, S., and Komander, D. (2019). Breaking the chains: deubiquitylating enzyme specificity begets function. *Nat. Rev. Mol. Cell Biol.* 20, 338–352.
- Faesen, A.C., Luna-Vargas, M.P., Geurink, P.P., Clerici, M., Merx, R., van Dijk, W.J., Hameed, D.S., El Oualid, F., Ova, H., and Sixma, T.K. (2011). The differential modulation of USP activity by internal regulatory domains, interactors and eight ubiquitin chain types. *Chem. Biol.* 18, 1550–1561.
- Finley, D. (2009). Recognition and processing of ubiquitin-protein conjugates by the proteasome. *Annu. Rev. Biochem.* 78, 477–513.
- Finley, D., Ulrich, H.D., Sommer, T., and Kaiser, P. (2012). The ubiquitin-proteasome system of *Saccharomyces cerevisiae*. *Genetics* 192, 319–360.
- Gao, Y., Li, Y., Zhang, C., Zhao, M., Deng, C., Lan, Q., Liu, Z., Su, N., Wang, J., Xu, F., et al. (2016). Enhanced purification of ubiquitinated proteins by engineered tandem hybrid ubiquitin-binding domains (ThUBDs). *Mol. Cell Proteomics* 15, 1381–1396.
- Gersch, M., Gladkova, C., Schubert, A.F., Michel, M.A., Maslen, S., and Komander, D. (2017). Mechanism and regulation of the Lys6-selective deubiquitinase USP30. *Nat. Struct. Mol. Biol.* 24, 920–930.
- Hershko, A., Ciechanover, A., and Varshavsky, A. (2000). Basic medical research award. The ubiquitin system. *Nat. Med.* 6, 1073–1081.
- Hoeller, D., and Dikic, I. (2009). Targeting the ubiquitin system in cancer therapy. *Nature* 458, 438–444.

- Huang, H., Jeon, M.S., Liao, L., Yang, C., Elly, C., Yates, J.R., 3rd, and Liu, Y.C. (2010). K33-linked polyubiquitination of T cell receptor-zeta regulates proteolysis-independent T cell signaling. *Immunity* 33, 60–70.
- Husnjak, K., and Dikic, I. (2012). Ubiquitin-binding proteins: decoders of ubiquitin-mediated cellular functions. *Annu. Rev. Biochem.* 81, 291–322.
- Ikeda, F., and Dikic, I. (2008). Atypical ubiquitin chains: new molecular signals. 'Protein Modifications: beyond the Usual Suspects' review series. *EMBO Rep.* 9, 536–542.
- Juang, Y.C., Landry, M.C., Sanches, M., Vittal, V., Leung, C.C., Ceccarelli, D.F., Mateo, A.R., Pruneda, J.N., Mao, D.Y., Szilard, R.K., et al. (2012). OTUB1 co-opts Lys48-linked ubiquitin recognition to suppress E2 enzyme function. *Mol. Cell* 45, 384–397.
- Kee, Y., Lyon, N., and Huibregtse, J.M. (2005). The Rsp5 ubiquitin ligase is coupled to and antagonized by the Ubp2 deubiquitinating enzyme. *EMBO J.* 24, 2414–2424.
- Kee, Y., Munoz, W., Lyon, N., and Huibregtse, J.M. (2006). The deubiquitinating enzyme Ubp2 modulates Rsp5-dependent Lys63-linked polyubiquitin conjugates in *Saccharomyces cerevisiae*. *J. Biol. Chem.* 281, 36724–36731.
- Kim, W., Bennett, E.J., Huttlin, E.L., Guo, A., Li, J., Possemato, A., Sowa, M.E., Rad, R., Rush, J., Comb, M.J., et al. (2011). Systematic and quantitative assessment of the ubiquitin-modified proteome. *Mol. Cell* 44, 325–340.
- Komander, D., and Rape, M. (2012). The ubiquitin code. *Annu. Rev. Biochem.* 81, 203–229.
- Kristariyanto, Y.A., Abdul Rehman, S.A., Weidlich, S., Knebel, A., and Kulathu, Y. (2017). A single MIU motif of MINDY-1 recognizes K48-linked polyubiquitin chains. *EMBO Rep.* 18, 392–402.
- Kulathu, Y., and Komander, D. (2012). Atypical ubiquitylation - the unexplored world of polyubiquitin beyond Lys48 and Lys63 linkages. *Nat. Rev. Mol. Cell Biol.* 13, 508–523.
- Li, Y., Dammer, E.B., Gao, Y., Lan, Q., Villamil, M.A., Duong, D.M., Zhang, C., Ping, L., Lauinger, L., Flick, K., et al. (2019). Proteomics links ubiquitin chain topology change to transcription factor Activation. *Mol. Cell* 76, 126–137.
- Ma, J., Chen, T., Wu, S., Yang, C., Bai, M., Shu, K., Li, K., Zhang, G., Jin, Z., He, F., et al. (2019). iProX: an integrated proteome resource. *Nucleic Acids Res.* 47, D1211–D1217.
- Mevissen, T.E.T., Hospenthal, M.K., Geurink, P.P., Elliott, P.R., Akutsu, M., Arnaudo, N., Ekkebus, R., Kulathu, Y., Wauer, T., El Oualid, F., et al. (2013). OTU deubiquitinases reveal mechanisms of linkage specificity and enable ubiquitin chain restriction analysis. *Cell* 154, 169–184.
- Mevissen, T.E.T., and Komander, D. (2017). Mechanisms of deubiquitinase specificity and regulation. *Annu. Rev. Biochem.* 86, 159–192.
- Min, M., Mevissen, T.E., De Luca, M., Komander, D., and Lindon, C. (2015). Efficient APC/C substrate degradation in cells undergoing mitotic exit depends on K11 ubiquitin linkages. *Mol. Biol. Cell* 26, 4325–4332.
- Nijman, S.M.B., Luna-Vargas, M.P.A., Velds, A., Brummelkamp, T.R., Dirac, A.M.G., Sixma, T.K., and Bernards, R. (2005). A genomic and functional inventory of deubiquitinating enzymes. *Cell* 123, 773–786.
- Ossareh-Nazari, B., Bonizec, M., Cohen, M., Dokudovskaya, S., Delalande, F., Schaeffer, C., Van Dorsselaer, A., and Dargemont, C. (2010). Cdc48 and Ufd3, new partners of the ubiquitin protease Ubp3, are required for ribophagy. *EMBO Rep.* 11, 548–554.
- Peng, J., Schwartz, D., Elias, J.E., Thoreen, C.C., Cheng, D., Marsischky, G., Roelofs, J., Finley, D., and Gygi, S.P. (2003). A proteomics approach to understanding protein ubiquitination. *Nat. Biotechnol.* 21, 921–926.
- Raman, M., Sergeev, M., Garnaas, M., Lydeard, J.R., Huttlin, E.L., Goessling, W., Shah, J.V., and Harper, J.W. (2015). Systematic proteomics of the VCP-UBXD adaptor network identifies a role for UBXN10 in regulating ciliogenesis. *Nat. Cell Biol.* 17, 1356–1369.
- Reyes-Turcu, F.E., Ventii, K.H., and Wilkinson, K.D. (2009). Regulation and cellular roles of ubiquitin-specific deubiquitinating enzymes. *Annu. Rev. Biochem.* 78, 363–397.
- Ritorto, M.S., Ewan, R., Perez-Oliva, A.B., Knebel, A., Buhlage, S.J., Wightman, M., Kelly, S.M., Wood, N.T., Virdee, S., Gray, N.S., et al. (2014). Screening of DUB activity and specificity by MALDI-TOF mass spectrometry. *Nat. Commun.* 5, 4763.
- Silva, G.M., Finley, D., and Vogel, C. (2015). K63 polyubiquitination is a new modulator of the oxidative stress response. *Nat. Struct. Mol. Biol.* 22, 116–123.
- Sims, J.J., and Cohen, R.E. (2009). Linkage-specific avidity defines the lysine 63-linked polyubiquitin-binding preference of rap80. *Mol. Cell* 33, 775–783.
- Sims, J.J., Haririnia, A., Dickinson, B.C., Fushman, D., and Cohen, R.E. (2009). Avid interactions underlie the Lys63-linked polyubiquitin binding specificities observed for UBA domains. *Nat. Struct. Mol. Biol.* 16, 883–889.
- Spence, J., Sadis, S., Haas, A.L., and Finley, D. (1995). A ubiquitin mutant with specific defects in DNA repair and multiubiquitination. *Mol. Cell Biol.* 15, 1265–1273.
- Stolz, A., and Dikic, I. (2018). Heterotypic ubiquitin chains: seeing is believing. *Trends Cell Biol.* 28, 1–3.
- Swaney, D.L., Beltrao, P., Starita, L., Guo, A., Rush, J., Fields, S., Krogan, N.J., and Villen, J. (2013). Global analysis of phosphorylation and ubiquitylation cross-talk in protein degradation. *Nat. Methods* 10, 676–682.
- Tong, Z., Kim, M.S., Pandey, A., and Espenshade, P.J. (2014). Identification of candidate substrates for the Golgi Tul1 E3 ligase using quantitative diGly proteomics in yeast. *Mol. Cell Proteomics* 13, 2871–2882.
- Udeshi, N.D., Svinkina, T., Mertins, P., Kuhn, E., Mani, D.R., Qiao, J.W., and Carr, S.A. (2013). Refined preparation and use of anti-diglycine remnant (K-epsilon-GG) antibody enables routine quantification of 10,000s of ubiquitination sites in single proteomics experiments. *Mol. Cell Proteomics* 12, 825–831.
- Wang, Q., Liu, X., Cui, Y., Tang, Y., Chen, W., Li, S., Yu, H., Pan, Y., and Wang, C. (2014). The E3 ubiquitin ligase AMFR and INSIG1 bridge the activation of TBK1 kinase by modifying the adaptor STING. *Immunity* 41, 919–933.
- Xiao, W., Liu, Z., Luo, W., Gao, Y., Chang, L., Li, Y., and Xu, P. (2020). Specific and unbiased detection of polyubiquitination via a sensitive non-antibody approach. *Anal. Chem.* 92, 1074–1080.
- Xu, P., Duong, D.M., Seyfried, N.T., Cheng, D., Xie, Y., Robert, J., Rush, J., Hochstrasser, M., Finley, D., and Peng, J. (2009). Quantitative proteomics reveals the function of unconventional ubiquitin chains in proteasomal degradation. *Cell* 137, 133–145.
- Yuan, W.C., Lee, Y.R., Lin, S.Y., Chang, L.Y., Tan, Y.P., Hung, C.C., Kuo, J.C., Liu, C.H., Lin, M.Y., Xu, M., et al. (2014). K33-Linked polyubiquitination of coronin 7 by cul3-KLHL20 ubiquitin E3 ligase regulates protein trafficking. *Mol. Cell* 54, 586–600.
- Zhu, D., Wang, Z., Zhao, J.J., Calimeri, T., Meng, J., Hideshima, T., Fulciniti, M., Kang, Y., Ficarro, S.B., Tai, Y.T., et al. (2015). The Cyclophilin A-CD147 complex promotes the proliferation and homing of multiple myeloma cells. *Nat. Med.* 21, 572–580.
- Zhuang, M., Guan, S., Wang, H., Burlingame, A.L., and Wells, J.A. (2013). Substrates of IAP ubiquitin ligases identified with a designed orthogonal E3 ligase, the NEDDylator. *Mol. Cell* 49, 273–282.

iScience, Volume 23

## **Supplemental Information**

### **Ubiquitin Linkage Specificity of Deubiquitinases**

#### **Determines Cyclophilin Nuclear**

#### **Localization and Degradation**

**Yanchang Li, Qiuyan Lan, Yuan Gao, Cong Xu, Zhongwei Xu, Yihao Wang, Lei Chang, Junzhu Wu, Zixin Deng, Fuchu He, Daniel Finley, and Ping Xu**

## Supplemental Figures and Legends

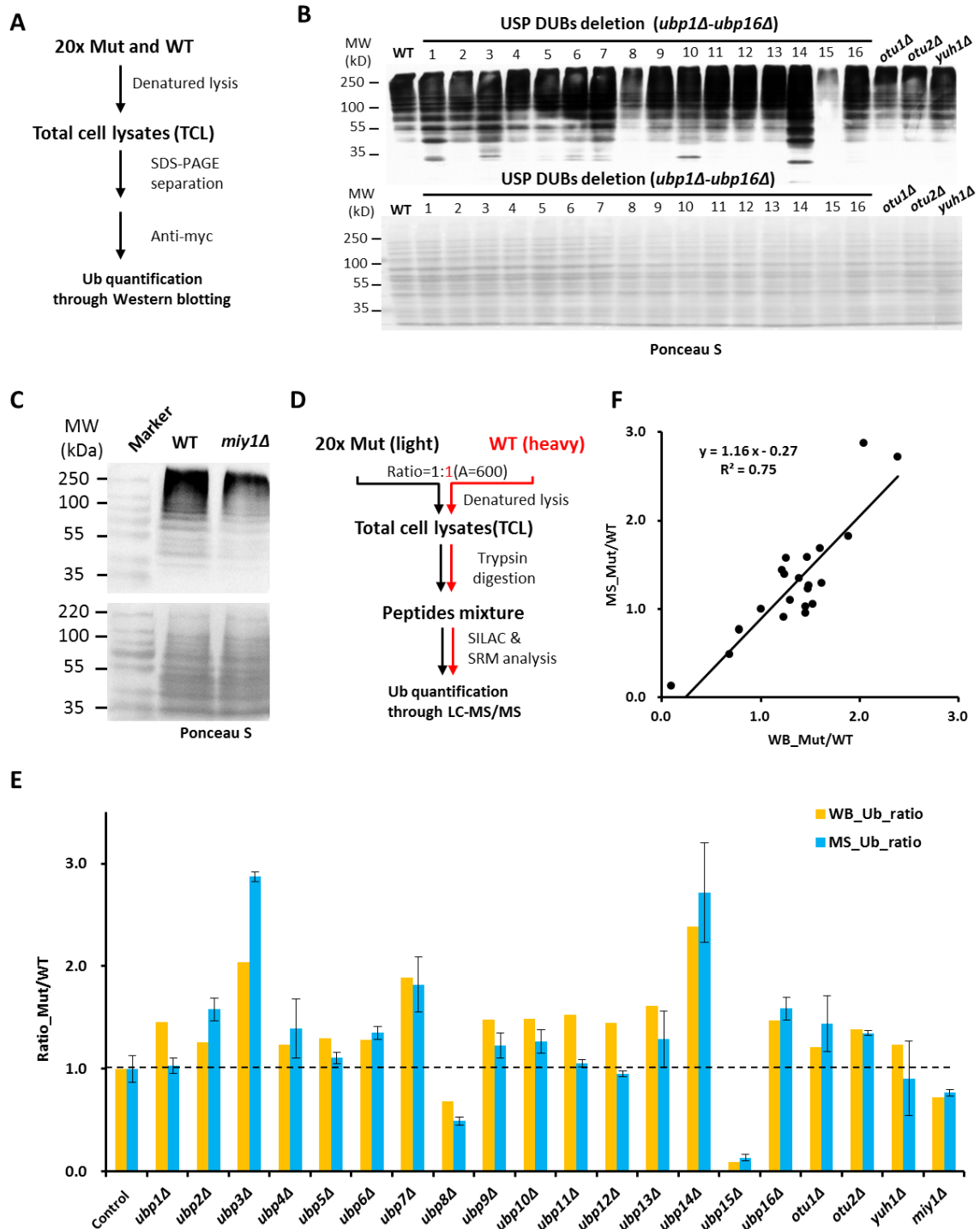


**Figure S1. Accumulation of Ub signal varies in different DUB deletion strains, Related to Figure 1.**

(A) Workflow for systematic evaluation of the ubiquitination signal through Western

blotting with TCL prepared from all of DUB deletion and WT strains. Equal amounts of yeast cells were used for comparison.

**(B)** Systematic evaluation of the ubiquitination signal through western blotting analysis. Same amounts of TCL from WT and mutant strains were resolved by SDS-PAGE and probed with anti-myc antibody. The experiment was repeated twice with the same trend. Ponceau S was set as loading control.

**(C)** The ubiquitination signal of the newly identified MINDY DUB Miy1 was measured as above. Same amounts of TCL from WT and Miy1 deletion strains were resolved by SDS-PAGE and probed with anti-myc antibody. The experiment was repeated twice with the same trend. Ponceau S was set as loading control.

**(D)** Workflow for systematic evaluation of the ubiquitination signal through SILAC quantification on TCL level. Same amounts of yeast cells from each individual mutant strains were equally mixed with heavy isotope labeled WT and digested with trypsin for further LC-MS/MS analysis.

**(E)** Fold change comparison of the ubiquitination signal from WB (Yellow bars) and MS (Blue bars) analysis. The dotted line stands for quantification of equal light and heavy WT cells.

**(F)** The correlation of the WB and MS quantification results was high and the  $R^2$  reaches up to 0.75.

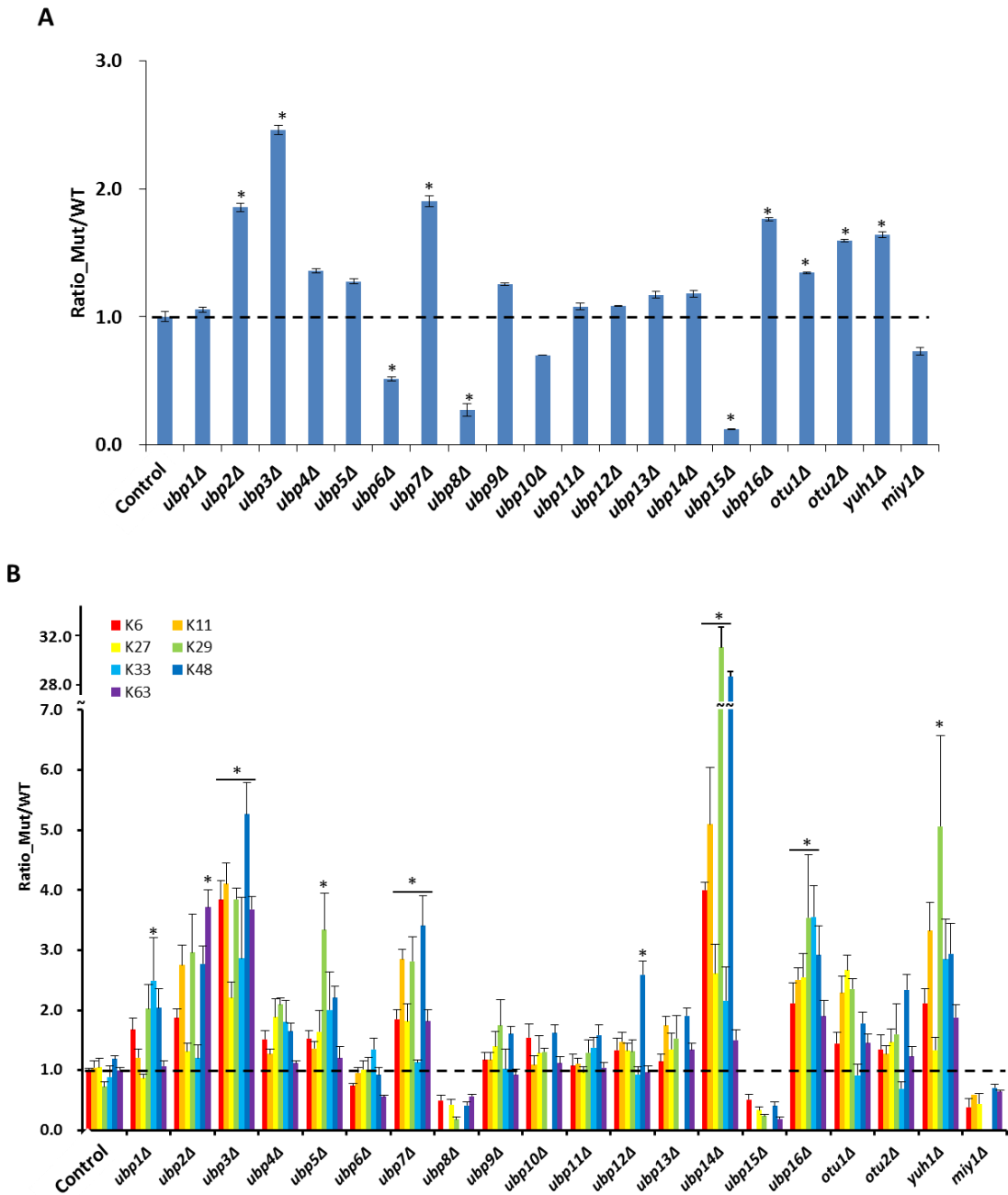


**Figure S2. The component of Ub-linkages varies in different DUB deletion strains, Related to Figure 1.**

(A) Comparison of the mono ubiquitin from <10 kDa section between DUB mutants and WT strains based on SILAC quantification. The control experiment represents the quantification variation of the platform with the WT (light) and WT (heavy) equally mixed. Two replicates were performed. Data shown as the mean  $\pm$  SEM.

(B) Comparison of ubiquitination level from the 10-50 kDa section between DUB mutants and WT strains based on SILAC quantification. Two replicates were

performed. Data shown as the mean  $\pm$  SEM. The asterisk for significantly increased chains passed *t* test (*p*-value < 0.05).

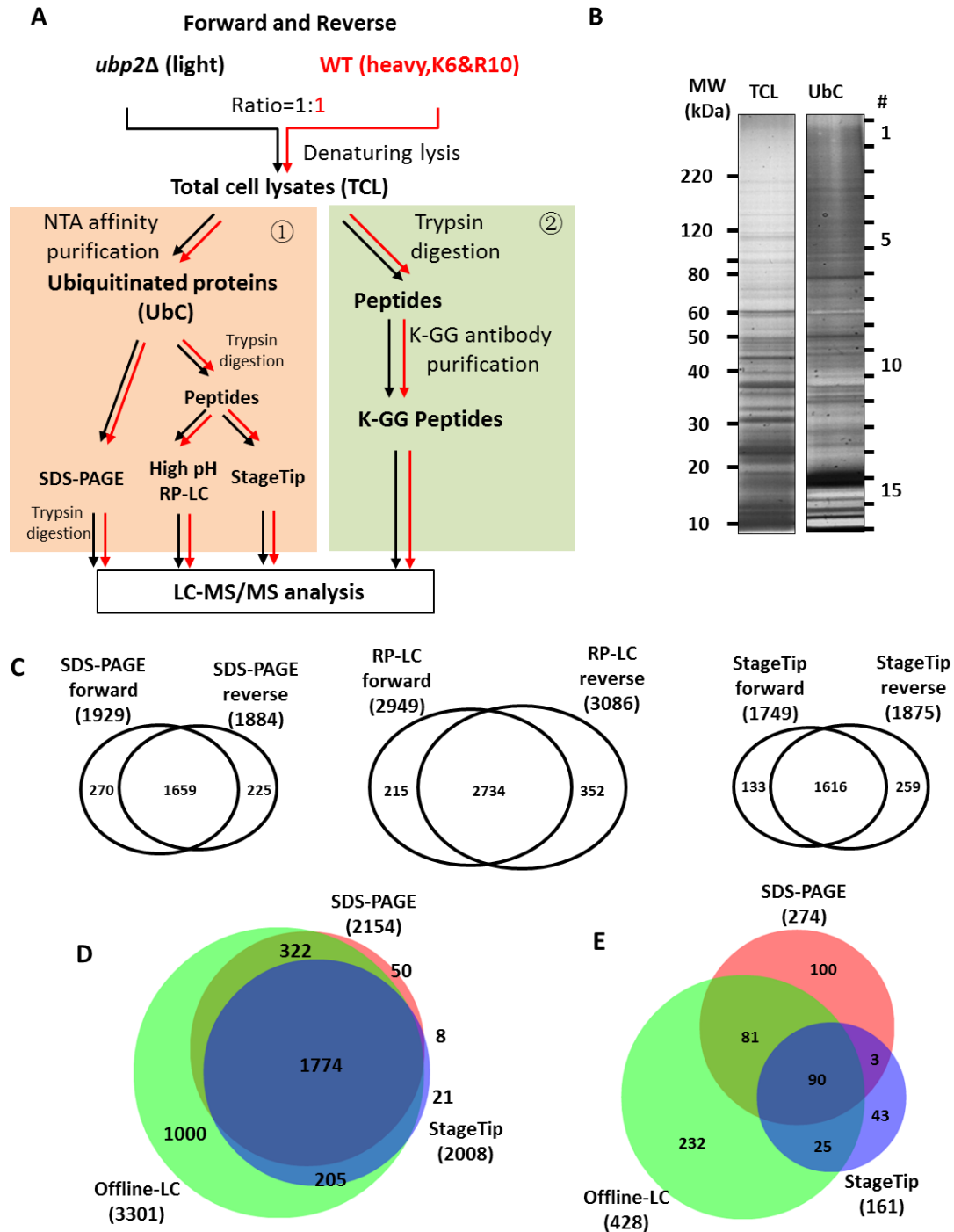


**Figure S3. High ubiquitome coverage is achieved for the DILUS strategy used to screen for Ubp2-regulated substrates and sites potentially modified with K63-linked chains, Related to Figure 2.**

(A) Workflow of DILUS strategy to directly screen for Ubp2 substrates. Two methods were used to enrich the ubiquitinated proteins to increase the coverage. The first was the ubiquitinated conjugates (UbC) enrichment (left, pink background) and the second was K- $\epsilon$ -GG peptides enrichment using antibody (right, green background). SILAC label-swap experiments were applied for biological repeats. In forward SILAC experiment, the *ubp2* $\Delta$  was cultured in light SC medium and WT was cultured in SC medium containing heavy isotope labeled amino acid (K6 & R10). In reverse SILAC experiment, the labeling of *ubp2* $\Delta$  and WT were swapped. The UbC sample was separated with three strategies including SDS-PAGE, high pH RP-LC and StageTip.

(B) TCL and UbC were resolved by 10% SDS-PAGE and detected with silver staining.

(C) Three strategies used for the identification of UbC from SILAC swap-labeling samples. The overlaps of the identified proteins from forward and reverse samples of SDS-PAGE (left), off-line high pH RP-LC (middle) and StageTip separation (right).

(D) Comparison of identified proteins from the separation of SDS-PAGE, off-line LC and StageTip strategies. Totally 3380 potential ubiquitinated proteins were identified.

(E) Comparison of identified K- $\epsilon$ -GG sites from the separation of SDS-PAGE, off-line RP-LC and StageTip strategies. Totally 579 ubiquitinated sites were quantified.

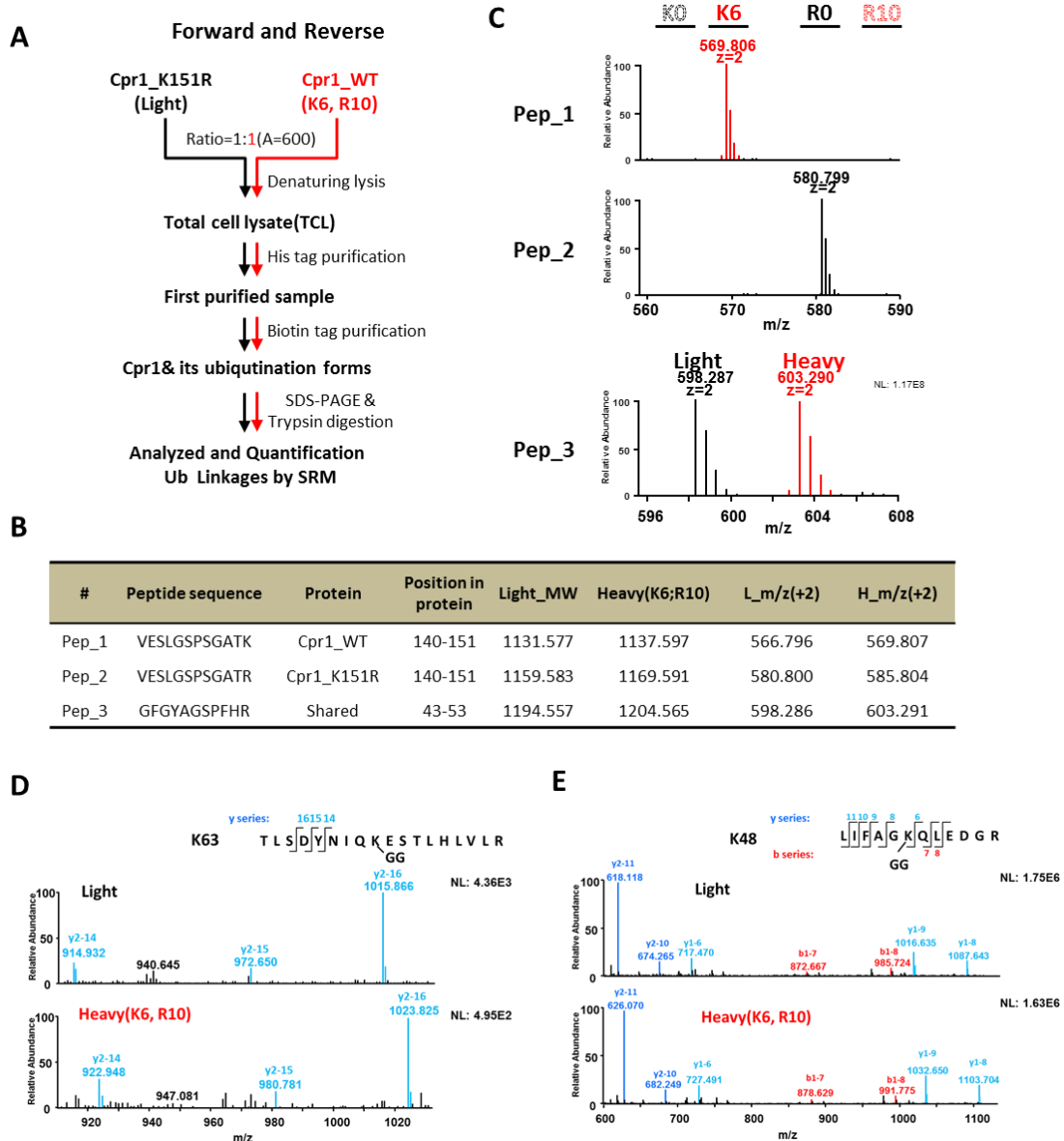


**Figure S4. SILAC quantification of ubiquitin chains on Cpr1 and Cpr1-K151R, Related to Figures 4 and 5.**

(A) Strategy for identification and quantification of ubiquitin chains on Cpr1 and Cpr1-K151R via swapped forward and reverse SILAC experiments. The forward experiment showed that the Cpr1-K151R and Cpr1 were cultured respectively in SC medium with light and heavy amino acid (K6 & R10). The reverse SILAC experiment swapped the labeling of Cpr1 and Cpr1-K151R in SC medium with light and heavy amino acid (K6 & R10). The two strains were mixed with equal amount of yeast cells. Then enriched the target proteins under tandem affinity purification in denatured condition. The resulting peptides were detected through SRM technology.

**(B)** Peptides list derived from Cpr1 and *Cpr1-K151R* for quantification. The pep\_1 (VESLGSPSGATK) and pep\_2 (VESLGSPSGATR) stands for unique peptides and pep\_3 (GFGYAGSPFHR) stands for shared peptide derived from Cpr1 and *Cpr1-K151R*.

**(C)** The three peptides quantification in forward experiment. The forward experiment consisted of light *Cpr1-K151R* and heavy Cpr1. There existed pep\_1 (heavy, red peaks) derived from heavy Cpr1 while there no light pep\_1. There existed pep\_2 (light, black peaks) derived from light *Cpr1-K151R* while there no heavy pep\_2. The shared peptide (pep\_3) derived from heavy Cpr1 and light *Cpr1-K151R* were appeared at the same time with similar intensity.

**(D)** Mass spectra of K63-linked K- $\epsilon$ -GG peptides identified on the purified HB-Cpr1 after trypsin digestion. The upper spectrum stands for light amino acid labeled derived from Cpr1 and the lower part for heavy isotope labeled from *Cpr1-K151R*.

**(E)** Mass spectra of K48-linked K- $\epsilon$ -GG peptides identified on the purified HB-Cpr1 after trypsin digestion. The upper spectrum stands for light amino acid labeled derived from Cpr1 and the lower part for heavy isotope labeled from *Cpr1-K151R*.

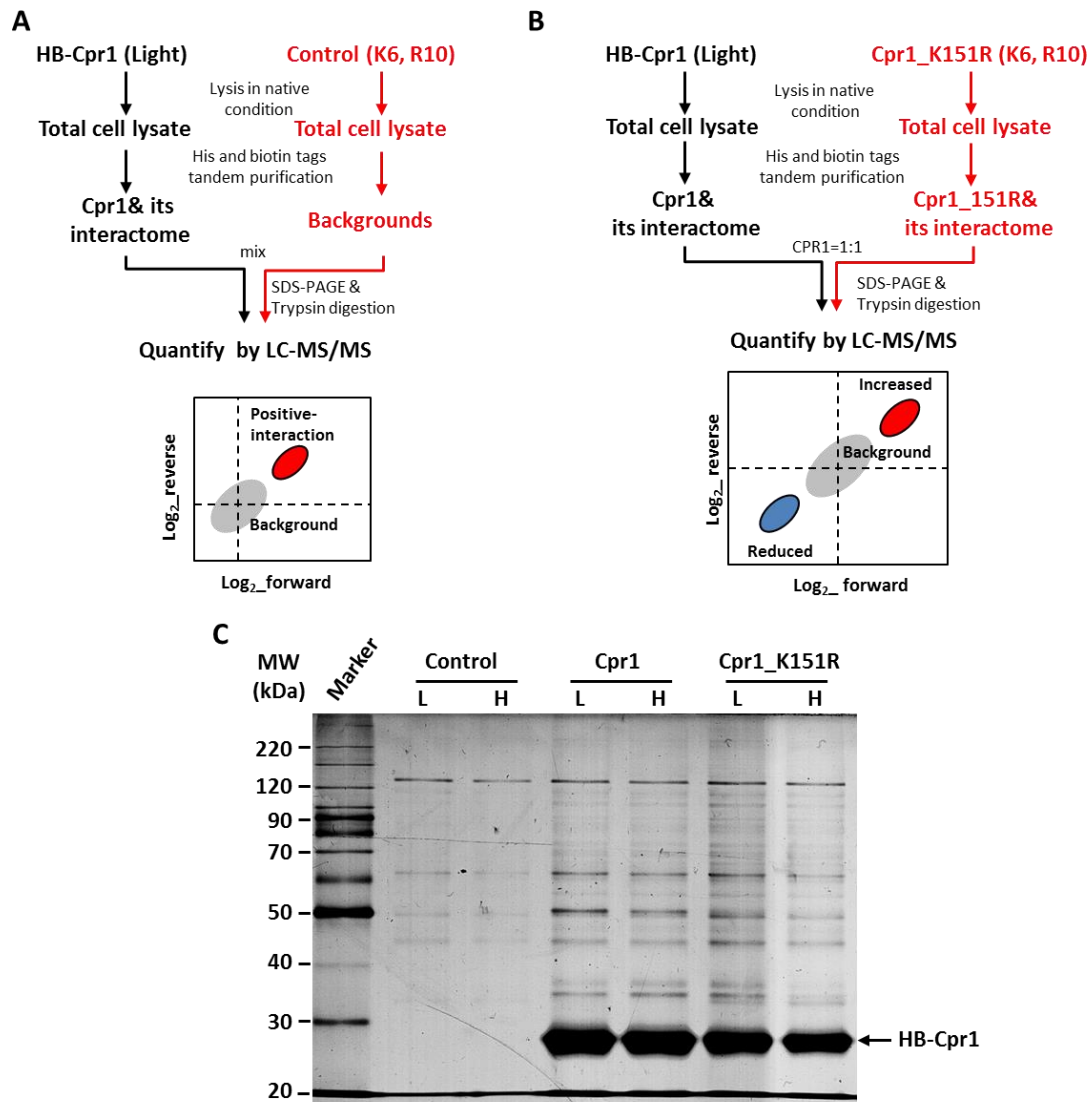


**Figure S5. Interactome profiling of Cpr1 and *Cpr1-K151R* purified from the native condition, Related to Figures 6 and 7.**

(A) Schematic diagram of interactome profiling for Cpr1 based on SILAC quantification. Forward and reverse swapped SILAC strategy was used for two biological replicates. The cell expressed blank vector was set as background control.

(B) Schematic diagram of interactome profiling targeting the K63-linked chain on Cpr1 based on SILAC quantification. Forward and reverse swapped SILAC strategy was used for two biological replicates. The cell expressed HB-Cpr1 was set as control.

(C) The control, Cpr1 and *Cpr1-K151R* strains were firstly labeled with light (L) and heavy (H) isotope amino acids. After tandem affinity purification and balanced through silver staining analysis, the samples were mixed according to the workflow mentioned

in panel A and B above.

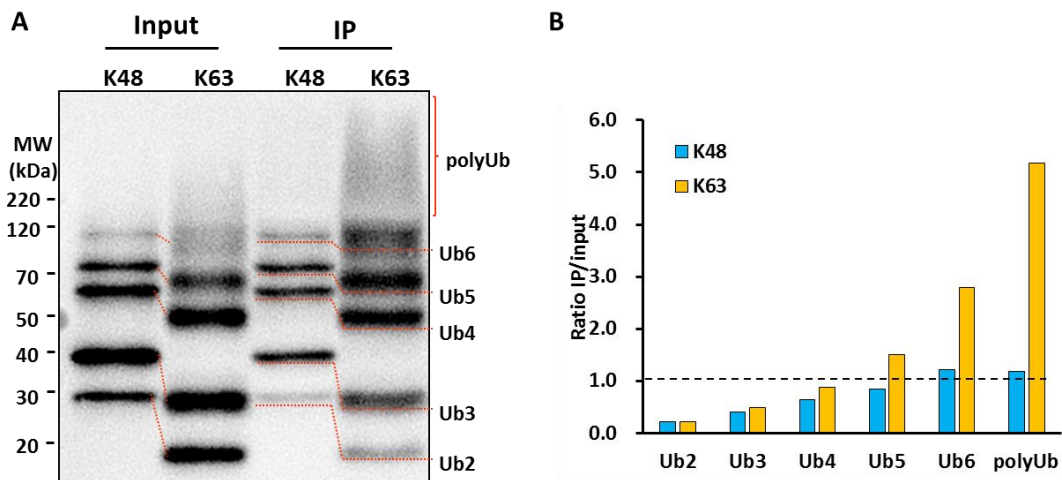


**Figure S6. Zpr1 interacts with K63-linked chain with higher affinity compared with K48-linked chain, Related to Figure 6.**

(A) The interaction analysis of the Zpr1 with K63- and K48-linked chains. Ubiquitin chains was 2-7 polymers. The detection of the chain signal was based on ThUBD by far-WB method (Xiao et al., 2020).

(B) The gray quantification comparison of K63- and K48-linked chains from panel A.

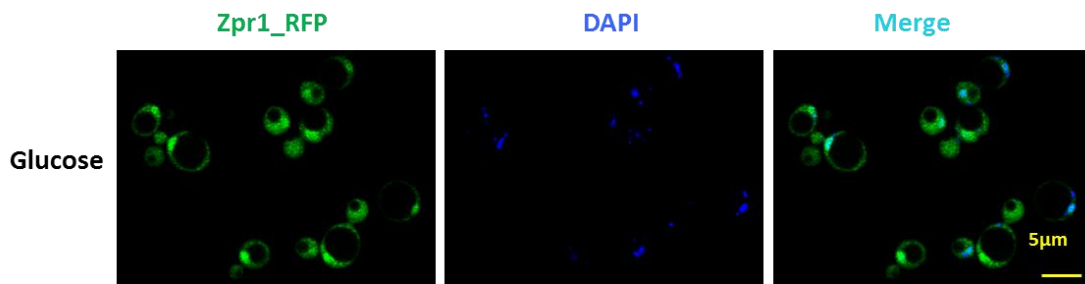


**Figure S7. Zpr1 re-localizes into nucleus under the stimulation of glucose, Related to Figure 6.**

The strain PXL033 expressing Zpr1-GFP were grown to log phase in YEPD medium, starved in glucose-free SC medium for 12 h, and then treated with glucose. The GFP (green) and DAPI (blue) represents Zpr1 and DNA, respectively (scale bar = 5 µm).

## Transparent Methods

### Strains, plasmids and protocols

Table S1 shows the yeast, *E.coli* and plasmids used in this study. All yeast strains were derived from strain JMP024 which expressed ubiquitin with polyhistidine and myc tags (Xu et al., 2009). In JMP024, all of the four endogenous ubiquitin genes were deleted, and a synthetic ubiquitin gene is expressed under the control of *CUP1* promoter in a 2 $\mu$  plasmid (Finley et al., 1994). Both the *LYS2* and *ARG4* genes were deleted for SILAC-labeling quantitative analysis (Xu et al., 2009).

To systematically evaluate the specificity of 7 lysine-linked ubiquitin linkages between deubiquitinating enzymes (DUBs), 20 of single DUB gene deletion strains (PXL005-PXL024) were constructed by homologous recombination on JMP024 background with kanamycin resistant gene separately (Li and Heyer, 2008). We could not generate *RPN11* deletion strain in this study, which might be essential for yeast viability (Amerik and Hochstrasser, 2004; Amerik et al., 2000).

To profile ubiquitin linkages on Cpr1 and its K151R mutant form, histidine (H) and biotin (B) tagged on C-terminal of Cpr1 and *Cpr1-K151R* expressed strains were constructed, respectively. HB tagged Cpr1 was obtained by fusing Cpr1 DNA fragment with the HB tag amplified from strain PY1226 (Tagwerker et al., 2006). Then the fused DNA construct was inserted into the pUB221 plasmid digested by Kpn I and Bgl II, resulting in plasmid pUB221-02 (**Table S1**). Cpr1 K151R site mutation was introduced into the pUB221-02 plasmid by QuickChange® II XL Site-Directed Mutagenesis Kit (Stratagene, La Jolla, CA) to generate pUB221-03 (**Table S1**). HB tagged Cpr1 and *Cpr1-K151R* mutant genes were both driven by *CUP1* promoter. pUB221-02 and pUB221-03 plasmids were transformed into JMP024, *ubp2* $\Delta$  and *ubp3* $\Delta$  strains (**Table S1**) with standard LiOAc method (Gietz and Woods, 2002). The Ubp2 catalytic site mutant (Ubp2 C745S) was introduced into JMP024 genome by fused a nourseothricin resistant gene at the C-terminal of Ubp2 C745S gene and constructed in the same way as mentioned above.

To determine the localization of Zpr1 and Cpr1 under the stimulus of glucose, the Zpr1-GFP and Cpr1-mcherry co-expressed strain PXL033 was constructed (**Table S1**). In addition, Zpr1-GFP with different Cpr1 mutation forms (*cpr1* $\Delta$  and *Cpr1-K151R*), ubiquitin K63R mutation, Ubp2 overexpressed and C745S mutant strains were constructed, respectively (**Table S1**). All fluorescent tags were on the C-terminal of the target genes and fused with a resistant gene as selection marker in JMP024 background (Huang and Hopper, 2014; Huh et al., 2003).

In general, yeast strains were cultured at 30 °C in YEPD medium (1% yeast extract, 2% Bacto-peptone, and 2% dextrose) until OD<sub>600</sub>=1.5 unless specified. For SILAC labeling, yeast cells were cultured in synthetic complete medium (SC) with light or heavy isotope amino acids (Geiger et al., 2011; Xu et al., 2009). To analyze the Ub linkages-mediated 26S proteasome degradation, the strain expressing HB-Cpr1 was inhibited with 50  $\mu$ M MG132 (**Figure 7F**) (Xu et al., 2009). For subcellular localization analysis, we cultured the strains in YEPD medium, and then replaced with synthetic complete medium without glucose to starve for 12 hours. Glucose was added to final concentration of 2% to stimulate the cells from quiescent to proliferating status (Ansari et al., 2002; Galcheva-Gargova et al., 1998).

### **Ubp2, Ubp3 and Zpr1 expression and purification**

To determine the specificity of Ubp2 and Ubp3 *in vitro*, recombinant expression was employed (Smith and Johnson, 1988). Ubp2 was PCR-amplified and inserted into the pCDFDuet-1 vector digested with EcoR I and Hind III, resulting in plasmid pCDFDuet-1.1. Ubp3 was PCR-amplified and inserted into the pET28b vector, resulting in plasmid pET28b-1.1(**Table S1**). The plasmid pCDFDuet-1.1 and pET28b-1.1 were transformed into *Escherichia coli* BL21 (DE3) resulting in PXE01 and PXE02 (**Table S1**). To overexpress the DUBs, the strain was induced with 1 mM isopropyl- $\beta$ -D-thiogalactopyranoside (IPTG) for 6 hours at 16 °C after OD<sub>600</sub> reached to 0.6. The harvested cells were lysed by sonication in lysis buffer (2 mM DTT, 150 mM NaCl in PBS), and purified the six histidine tagged protein using the Ni-NTA agarose (Xu et al., 2009). The protein was eluted by 60 mM imidazole and stored at 4 °C in PBS

supplemented with 10% glycerol for further usage. For analysis of the interaction between Zpr1 and ubiquitin chains, Zpr1 was expressed and purified in the same way mentioned above.

### **Proteomics analysis by SILAC**

Swapped SILAC-based strategies were used for global proteome quantitation, Ub linkage quantification, interactome profiling and so on to reduce the systematic variation and error. For SILAC culture, the detail protocols were described previously (Geiger et al., 2011; Xu et al., 2009). The SC medium (0.67% yeast nitrogen base, 2% glucose, and supplemented with the appropriate amino acids). The light medium contained natural arginine (20 mg/liter) and lysine (30 mg/liter), and the heavy medium contained equal molar amount of [ $^{13}\text{C}_6^{15}\text{N}_4$ ] arginine (R10, + 10.0083 Da) and [ $^{13}\text{C}_6$ ] lysine (K6, + 6.0201 Da) from the Cambridge Isotope Laboratories (Tewksbury, MA, USA). After harvested at the early exponential growth phase ( $\text{OD}_{600}=1.5$ ), the yeast cells were washed with precooled 0.1%  $\text{NaN}_3$  and stored at  $-80^\circ\text{C}$  for further usage.

The harvested yeast cells were lysed in denatured or native condition based on the subsequent experiment purpose. The denatured lysis buffer (8 M urea, 100 mM  $\text{Na}_2\text{HPO}_4$ , 10 mM Tris, 5 mM iodoacetamide, 1 mM PMSF, 5 mM *N*-ethylmaleimide, pH 8.0) was employed to protect the ubiquitination status and also reduce the purification background. The native lysis buffer (50 mM Tris, pH8.0, 150 mM NaCl, 1% NP-40, 5 mM iodoacetamide, 5% glycerol, 1 mM PMSF, 5 mM *N*-ethylmaleimide) was employed for Cpr1 interactome profiling as shown in Supplementary Figure 5.

The light and heavy labeled yeast cells were mixed at 1:1 ratio ( $\text{OD}_{600}$ ). Then cells were broken with glass beads for 15 cycles of 20s in a homogenizer (Bertin Technologies, France) and 1 min on ice to keep sample cool. Total cell lysate (TCL) was centrifuged at 10,000g for 5 min at  $4^\circ\text{C}$ . Proteins were reduced with 5 mM dithiothreitol (DTT) at room temperature for 30 min and alkylated with 15 mM iodoacetamide (IAA) in darkness for 30 min. Protein lysates were separated by 10% SDS-PAGE and sliced into 24 fractions based on sample complexity and molecular weight markers and digested with trypsin (Hualishi Tech, Beijing, China) overnight at

37°C. The tryptic peptides were extracted with extraction buffer (5% formic acid and 45% acetonitrile) and then acetonitrile, and finally dried using a vacuum dryer (LABCONCO CentriVap, Kansas City, USA).

### **Separation of ubiquitinated conjugates (UbC)**

To increase the coverage of UbC and ubiquitin modified peptides, three separation strategies were employed, including (I) SDS-PAGE, (II) off-line high pH reverse phase LC and (III) StageTip separation (**Figure S3**).

When separated with SDS-PAGE, the enriched UbC was separated with 10% SDS-PAGE followed by trypsin digestion and LC-MS/MS analysis.

To concentrate the ubiquitinated peptides to facilitate MS identification, the same batch of enriched UbC was digested with trypsin first and then separated with off-line high pH RP-LC with similar method as described previously (Ding et al., 2013; Peng et al., 2003; Xiao et al., 2019). Briefly the ubiquitinated peptides modified with di-Gly at lysine residue (K-ε-GG) was miscleaved and the retention time was delayed. Increasing the buffer B (0.1% FA in ACN) appropriately will reduce the interferences of unmodified peptides and increase the intensity of ubiquitinated peptides (Gao et al., 2016; Li et al., 2017).

To simplify the off-line LC separation procedure with tiny amounts of enriched UbC, we also developed StageTip based separation method for UbC separation on peptides level as well. Briefly, ~5 μg of tryptic peptides from UbC were loaded on the homemade StageTip column. After extensive wash, the bound peptides were eluted by stepwise increasing ACN concentration in elution buffer into 10 fractions before LC-MS analysis.

### **Enrichment of ubiquitin modified peptides with K-ε-GG antibody**

To further increase the coverage of ubiquitin modified peptides, K-ε-GG antibody was used for the modified peptides enrichment. SILAC-labeled cell pellets of WT and *ubp2Δ* were lysed in denaturing conditions as mentioned above. Protein concentrations were measured using a bicinchoninic acid (BCA) protein assay (Thermo Fisher Scientific, San Jose, CA, USA). About 10 mg of protein were input and reduced with 5

mM dithiothreitol DTT for 30 min at room temperature and subsequently carbamidomethylated using 15 mM IAA for 30 min at room temperature in the darkness. Lysates were then diluted to 4 M urea with 50 mM  $\text{NH}_4\text{HCO}_3$ , and digested for 4 hours at 37 °C with sequencing grade LysC (Promega, Madison, USA) at an enzyme to substrate ratio of 1:100. Following, samples were then diluted to 1 M urea with 50 mM  $\text{NH}_4\text{HCO}_3$ , and digested overnight at 37 °C with sequencing grade trypsin (Hualishi Tech, Beijing, China) at an enzyme to substrate ratio of 1:50. Then the samples were acidified with formic acid (FA) and subsequently desalted using a C18 Sep-Pak SPE cartridge (Waters, Milford Massachusetts, USA). Then the dried peptides were resuspended in 1.0 ml of IAP buffer and incubated with 20  $\mu\text{L}$  anti-K- $\epsilon$ -GG antibody beads (Cell Signaling Technology, Danvers, MA, USA) for 1 hour at 4 °C. Antibody beads were washed with 3-5 ml of cold PBS. The K- $\epsilon$ -GG peptides were eluted by adding 0.2% trifluoroacetic acetic (TFA). Peptide supernatants were desalted using C18 StageTip and separated into 3 fractions as mentioned above.

### **LC-MS/MS analysis**

The resulting peptides were analyzed on the LC-MS/MS platform of hybrid LTQ-Orbitrap Velos mass spectrometer (Thermo Fisher Scientific, San Jose, CA, USA) equipped with a Waters nanoACQUITY ultra performance liquid chromatography (UPLC) system (Waters, Milford, MA, USA). Peptides were separated on a 75  $\mu\text{m}$  I.D.  $\times$  15 cm capillary column (Beijing SpectraPeaks, Beijing, China) packed with 3  $\mu\text{m}$  C18 reverse-phase fused-silica (Michrom Bioresources, Inc., Auburn, CA, USA). The LC nonlinear gradient with 60 min ramped from 8% to 40% of mobile phase B (phase B: 0.1% FA in ACN, phase A: 0.1% FA+ 2% ACN in water) at a nano flow rate of 300 nL/min. The MS1 was detected with a mass range of 300–1,600 at a resolution of 30,000 at  $m/z$  400. The automatic gain control (AGC) was set as  $1 \times 10^6$  and the maximum injection time (MIT) was 150 ms. The MS2 was detected in data-dependent mode for the 20 most intense ions subjected to fragmentation in the linear ion trap (LTQ). For each scan, the AGC was set at  $1 \times 10^4$  and the MIT was set at 25 ms. The dynamic range was set at 30–45 s to suppress repeated detection of the same ion peaks.

## **MS data analysis for protein identification and quantification**

All the raw files were searched by MaxQuant (Cox and Mann, 2008) (version 1.5.30) against the Swiss-Prot reviewed yeast database (version 2013.10, containing 6652 entry proteins). For proteome identification, searching parameters consisted of full tryptic restriction and peptides were allowed up to two miss cleavages. Precursor mass tolerance was set at 20 ppm for the first search and 6 ppm for the main search. The tolerance of MS2 fragments was set at 0.5 Da. Peptide matches were filtered by a minimum length of seven amino acids. Carbamidomethylation of cysteine was specified as a fixed modification and oxidation of methionine was assigned as a variable modification. For ubiquitination identification, a re-search strategy was used that di-Gly-lysine was added in the second search (Gao et al., 2016; Peng et al., 2003). The peptides of C-terminal lysine modified residue with localization probability larger than 0.75 were removed from the dataset. The peptides, proteins and site identification were filtered with false discovery rate (FDR) lower than 1% using a target-decoy search strategy (Elias and Gygi, 2007; Eng et al., 1994).

For SILAC quantification, the labeled lysine (K6) and arginine (R10) were added as a variable modification. The labeling efficiency of heavy-isotope labeled lysine and arginine reached up to 99% in the yeast. At least two unique or razor peptides were required for protein quantification. Using the two or more replicate measurements for Ubp2 deletion condition, differentially (up or down) regulated peptides and proteins were identified using the moderated t-statistic. The standard errors are calculated using an empirical Bayes method utilizing information across all peptides, thereby making inference about each individual modified peptide and protein more robust. The *p* values arising from moderated t-statistics are corrected for multiple testing by controlling the false discovery rate (FDR), as proposed by Benjamini and Hochberg. Peptides and proteins with an FDR adjusted *p*-value of less than 0.1 and the fold change of  $\pm 1.5$  ( $\log_2FC$  at  $\pm 0.58$ ) were deemed to be significantly changed (Udeshi et al., 2012).

## **Functional and bioinformatics analysis of identified peptide and proteins**

Protein information, including gene symbol and modifications, was mainly generated from SGD annotations. Part of ubiquitination annotations came from database UUCD 2.0 (<http://uucd.biocuckoo.org/>) (Gao et al., 2013), GO Enrichment analysis was achieved by SGD (<http://www.yeastgenome.org/>) (Cherry et al., 1998). Venn was drawn by the online tool (<http://www.cmbi.ru.nl/cdd/biovenn/index.php#userconsent#>) (Hulsen et al., 2008).

## **Western blot assay**

Total cell lysates were prepared under denatured condition as mentioned above. Bound proteins were eluted with SDS-PAGE loading buffer (80 °C, 5min). The elution was subjected to standard immunoblot analysis for detection. The antibodies used in this study as indicated in figures, including anti-Ub-K63 antibody (EMD Millipore, Billerica, MA, USA, cat. no. 05-1308, clone apu3), anti-Ub-K48 antibody (EMD Millipore, cat. no. 05-1307, clone apu2), anti-c-myc antibody (Santa Cruz, cat. no. sc-40, 9E10), ubiquitin antibody (Santa Cruz, cat. no. sc-8017, P4D1), streptavidin antibody (Abcam, cat. no. ab1227) and GAPDH antibody (Abcam, cat. no. ab9485).

## **Tandem affinity purification (TAP)**

Tandem affinity purification was employed in this study to enrich target protein. Cells expressing HB-tagged *Cpr1* and *Cpr1-K151R* proteins were cultured to early exponential growth phase in SILAC-based medium or SC medium and purified in denatured or native condition based on the subsequent experiment purpose.

To measure the ubiquitin linkages on protein substrates, cells were lysed in denatured buffer A (8 M Urea, 50 mM Tris, 300 mM NaCl, 5 mM iodoacetamide, 5 mM imidazole, 0.5% Nonidet P-40, 10 mM PMSF and 10 mM *N*-ethylmaleimide, pH8.0). The clarified lysate was loaded onto a homemade nickel column (Qiagen, Valencia, CA) followed by washing with buffer A and then buffer B (buffer A plus 10mM imidazole). Bound proteins on nickel column were eluted by buffer C (8 M urea, 100 mM Tris, 200 mM NaCl, 150 mM imidazole, and 10mM EDTA, pH8.0). The elute was loaded onto a

pre-equilibrated homemade column packed with streptavidin beads (Invitrogen, Carlsbad, CA, USA) followed by washing with buffer D (8 M Urea, 100 mM Tris, 200 mM NaCl, 0.1% SDS, pH 8.0) and then buffer E (100 mM Tris, 200 mM NaCl and 0.1% SDS, pH 8.0) to remove the urea. Finally, the bound proteins were eluted by boiling the beads with 2x SDS Laemmli loading buffer (50 mM Tris-HCl, 2% SDS, 10% glycerol, 0.1% bromophenol blue, 1%  $\beta$ -mercaptoethanol, pH6.8) at 80°C for 10 min.

For native condition interactome profiling (**Figure S5**), the procedures were essentially the same as that of denatured conditions described above except the buffer component. Buffer A includes 50mM  $\text{NaH}_2\text{PO}_4$ , 150 mM NaCl, 1% Triton X-100, 10% glycerol, 5 mM imidazole, 2 mM  $\beta$ - mercaptoethanol, 10 mM PMSF and 10 mM *N*-ethylmaleimide. Buffer B contains 50 mM  $\text{NaH}_2\text{PO}_4$ , 150 mM NaCl, 0.5% Triton X-100, 10% glycerol, 10 mM imidazole, 2 mM  $\beta$ - mercaptoethanol, 5 mM iodoacetamide. Buffer C was made with buffer B supplemented with 0.5 M imidazole. Buffer D was made with buffer B without  $\beta$ - mercaptoethanol and imidazole. Buffer E contains 50 mM  $\text{NaH}_2\text{PO}_4$  and 150 mM NaCl. Finally, the bound proteins were eluted by boiling with 2x SDS Laemmli loading buffer (50 mM Tris-HCl, 2% SDS, 10% glycerol, 0.1% bromophenol blue, 1%  $\beta$ -mercaptoethanol, pH6.8) at 80°C for 10min.

### **Quantitative mass spectrometry analysis of selected proteins and Ub linkages**

The quantification of Ub and polyUb linkages on HB-Cpr1 or *HB-Cpr1-K151R* was performed with metabolically labeled cells/proteins as internal standard. We applied swapped SILAC to minimize variations during sample preparation (Xu et al., 2009). To measure the constitution and the abundance of ubiquitin linkages modified on HB-Cpr1, swapped SILAC strategy was applied (**Figure S4**). HB-Cpr1 and *HB-Cpr1-K151R* labeled with light and heavy isotope labeled amino acids respectively were mixed equally. After tandem affinity purification in denatured condition, the sample was digested with trypsin overnight. The resulting peptide samples were dissolved in a MS sample resuspending buffer (1% FA, 1% ACN) and analyzed by LC-MS platform mentioned above. Eluted peptides were detected by the Orbitrap mass spectrometer in a survey scan (300–1600 m/z, resolution 30,000) followed by selective reaction

monitoring (SRM) scans in the LTQ for seven ubiquitin linkages (Xiao et al., 2019; Xu et al., 2006; Xu et al., 2009). The intensities of peptides were manually analyzed by ion chromatograms using Xcalibur v2.0 software (Thermo Finnigan, San Jose, CA, USA).

### ***In vitro* deubiquitination assays of Ubp2 and Ubp3**

The Ubp2 and Ubp3 purified under native condition were quality checked and quantified through SDS-PAGE followed by Coomassie brilliant blue staining. The deubiquitination assay was performed as described (Hospenthal et al., 2015; Mevissen et al., 2013). In briefly, a 5 × reaction buffer is prepared containing 250 mM NaCl, 250 mM Tris (pH 7.5) and 25 mM DTT. To inhibit the DUB activity, 10 mM *N*-ethylmaleimide (NEM) was applied (Figure 1F and 7E). Then the Ubp2 or Ubp3 was mixed with the reaction buffer and incubated for 10 minutes at 37°C. After the activation of Ubp2 and Ubp3, about 0.2 µg K48 and K63-linked diUb were mixed with reaction buffer respectively and incubated at 37°C within 30 min. The reaction was ended with SDS Laemmli loading buffer followed by separation on a 15% SDS-PAGE and probing with anti-ubiquitin antibody or ThUBD.

### ***In vitro* interaction assays of Zpr1 with K48- and K63-linked ubiquitin chains**

Equal amounts of Ni-NTA beads bounded Zpr1 was incubated with K48- and K63-linked ubiquitin chains, respectively. After rotation slowly at 4 °C for 1h, the beads was washed with 1ml PBS six times. The bounded protein was eluted by 2x SDS Laemmli loading buffer at 80 °C for 5 min. The ubiquitin chains interacted with Zpr1 were detected by far western blot with ThUBD, which was unbiased for both K48- and K63-linked chains. The nitrocellulose (NC) membrane which had transferred protein onto it was incubated with GST-tagged ThUBD for 2h, and then incubated with primary anti-GST antibody and anti-mouse secondary antibody stepwise. The signal of ubiquitin chains were analysis by usual ECL fluid.

### **GFP and mCherry confocal fluorescence microscopy analysis**

The strains expressing GFP-Zpr1 respectively with Cpr1, *cpr1*Δ, *Cpr1-K151R*, Ub-K63R, and Ubp2 C745S mutant were grown in SC medium to early-exponential

phase ( $A_{600}=0.7$ ) and then washed three times with SC medium without glucose. The strains were starved overnight in glucose-free SC medium and then induced for one hour after supplementing with 2% glucose. Cells were washed with ddH<sub>2</sub>O and then visualized with a ZEISS LSM880 confocal fluorescence microscope with 60x objective (ZEISS, Oberkochen, Germany). GFP was excited with a 488 nm laser, and its emission was collected at 509 nm, while mCherry was excited with a 555 nm laser and its emission was collected at 577 nm (Huang and Hopper, 2014).

### **Data collection and database construction**

Supplemental Data include Supplemental Experimental Procedures and Results, 7 figures, and 7 tables, which can be found with this article online. The MS raw data have been upload and deposited on proteomeXchange (<http://www.proteomexchange.org/>) with the identifier PXD017357 and iProX (<https://www.iprox.org/>) with identifier IPX0001986000.

### **Supplemental References**

- Amerik, A.Y., and Hochstrasser, M. (2004). Mechanism and function of deubiquitinating enzymes. *Biochim Biophys Acta* 1695, 189-207.
- Amerik, A.Y., Li, S.J., and Hochstrasser, M. (2000). Analysis of the deubiquitinating enzymes of the yeast *Saccharomyces cerevisiae*. *Biol Chem* 381, 981-992.
- Ansari, H., Greco, G., and Luban, J. (2002). Cyclophilin A peptidyl-prolyl isomerase activity promotes ZPR1 nuclear export. *Mol Cell Biol* 22, 6993-7003.
- Cherry, J.M., Adler, C., Ball, C., Chervitz, S.A., Dwight, S.S., Hester, E.T., Jia, Y., Juvik, G., Roe, T., Schroeder, M., *et al.* (1998). SGD: *Saccharomyces* Genome Database. *Nucleic Acids Res* 26, 73-79.
- Cox, J., and Mann, M. (2008). MaxQuant enables high peptide identification rates, individualized p.p.b.-range mass accuracies and proteome-wide protein quantification. *Nat Biotechnol* 26, 1367-1372.
- Ding, C., Jiang, J., Wei, J., Liu, W., Zhang, W., Liu, M., Fu, T., Lu, T., Song, L., Ying, W., *et al.* (2013). A fast workflow for identification and quantification of proteomes. *Mol Cell Proteomics* 12, 2370-2380.
- Elias, J.E., and Gygi, S.P. (2007). Target-decoy search strategy for increased confidence in large-scale protein identifications by mass spectrometry. *Nat Methods* 4, 207-214.
- Eng, J.K., McCormack, A.L., and Yates, J.R. (1994). An approach to correlate tandem mass spectral data of peptides with amino acid sequences in a protein database. *J Am Soc Mass Spectrom* 5, 976-989.
- Finley, D., Sadis, S., Monia, B.P., Boucher, P., Ecker, D.J., Crooke, S.T., and Chau, V. (1994). Inhibition of proteolysis and cell cycle progression in a multiubiquitination-deficient yeast mutant. *Mol Cell Biol* 14, 5501-5509.

Galcheva-Gargova, Z., Gangwani, L., Konstantinov, K.N., Mikrut, M., Theroux, S.J., Enoch, T., and Davis, R.J. (1998). The cytoplasmic zinc finger protein ZPR1 accumulates in the nucleolus of proliferating cells. *Mol Biol Cell* *9*, 2963-2971.

Gao, T., Liu, Z., Wang, Y., Cheng, H., Yang, Q., Guo, A., Ren, J., and Xue, Y. (2013). UUCD: a family-based database of ubiquitin and ubiquitin-like conjugation. *Nucleic Acids Res* *41*, D445-451.

Gao, Y., Li, Y., Zhang, C., Zhao, M., Deng, C., Lan, Q., Liu, Z., Su, N., Wang, J., Xu, F., *et al.* (2016). Enhanced Purification of Ubiquitinated Proteins by Engineered Tandem Hybrid Ubiquitin-binding Domains (ThUBDs). *Mol Cell Proteomics* *15*, 1381-1396.

Geiger, T., Wisniewski, J.R., Cox, J., Zanivan, S., Kruger, M., Ishihama, Y., and Mann, M. (2011). Use of stable isotope labeling by amino acids in cell culture as a spike-in standard in quantitative proteomics. *Nat Protoc* *6*, 147-157.

Gietz, R.D., and Woods, R.A. (2002). Transformation of yeast by lithium acetate/single-stranded carrier DNA/polyethylene glycol method. *Methods Enzymol* *350*, 87-96.

Hospenthal, M.K., Mevissen, T.E., and Komander, D. (2015). Deubiquitinase-based analysis of ubiquitin chain architecture using Ubiquitin Chain Restriction (UbiCRest). *Nat Protoc* *10*, 349-361.

Huang, H.Y., and Hopper, A.K. (2014). Separate responses of karyopherins to glucose and amino acid availability regulate nucleocytoplasmic transport. *Mol Biol Cell* *25*, 2840-2852.

Huh, W.K., Falvo, J.V., Gerke, L.C., Carroll, A.S., Howson, R.W., Weissman, J.S., and O'Shea, E.K. (2003). Global analysis of protein localization in budding yeast. *Nature* *425*, 686-691.

Hulsen, T., de Vlieg, J., and Alkema, W. (2008). BioVenn - a web application for the comparison and visualization of biological lists using area-proportional Venn diagrams. *BMC Genomics* *9*, 488.

Li, X., and Heyer, W.D. (2008). Homologous recombination in DNA repair and DNA damage tolerance. *Cell Res* *18*, 99-113.

Li, Y., Wang, Z., Zhou, W., Zhang, K., Ma, J., Wu, F., Ji, J., Hong, X., Deng, Z., He, S., *et al.* (2017). A rapid and easy protein N-terminal profiling strategy using (N-Succinimidyl)oxycarbonylmethyltris(2,4,6-trimethoxyphenyl)phosphonium bromide (TMPP) labeling and StageTip. *Proteomics* *17*.

Mevissen, Tycho E.T., Hospenthal, Manuela K., Geurink, Paul P., Elliott, Paul R., Akutsu, M., Arnaudo, N., Ekkebus, R., Kulathu, Y., Wauer, T., El Oualid, F., *et al.* (2013). OTU Deubiquitinases Reveal Mechanisms of Linkage Specificity and Enable Ubiquitin Chain Restriction Analysis. *Cell* *154*, 169-184.

Peng, J., Schwartz, D., Elias, J.E., Thoreen, C.C., Cheng, D., Marsischky, G., Roelofs, J., Finley, D., and Gygi, S.P. (2003). A proteomics approach to understanding protein ubiquitination. *Nat Biotechnol* *21*, 921-926.

Smith, D.B., and Johnson, K.S. (1988). Single-step purification of polypeptides expressed in *Escherichia coli* as fusions with glutathione S-transferase. *Gene* *67*, 31-40.

Tagwerker, C., Flick, K., Cui, M., Guerrero, C., Dou, Y., Auer, B., Baldi, P., Huang, L., and Kaiser, P. (2006). A tandem affinity tag for two-step purification under fully denaturing conditions: application in ubiquitin profiling and protein complex identification combined with in vivocross-linking. *Mol Cell Proteomics* *5*, 737-748.

Udeshi, N.D., Mani, D.R., Eisenhaure, T., Mertins, P., Jaffe, J.D., Clauser, K.R., Hacohen, N., and Carr, S.A. (2012). Methods for quantification of in vivo changes in protein ubiquitination following proteasome and deubiquitinase inhibition. *Mol Cell Proteomics* *11*, 148-159.

Xiao, W., Liu, Z., Luo, W., Gao, Y., Chang, L., Li, Y., and Xu, P. (2020). Specific and Unbiased Detection of Polyubiquitination via a Sensitive Non-Antibody Approach. *Anal Chem* *92*, 1074-1080.

Xiao, W., Zhang, J., Wang, Y., Liu, Z., Wang, F., Sun, J., Chang, L., Xia, Z., Li, Y., and Xu, P. (2019). Ac-LysargiNase Complements Trypsin for the Identification of Ubiquitinated Sites. *Anal Chem* *91*, 15890-15898.

Xu, P., Cheng, D., Duong, D.M., Rush, J., Roelofs, J., Finley, D., and Peng, J. (2006). A proteomic strategy for quantifying polyubiquitin chain topologies. *Israel Journal of Chemistry* *46*, 171-182.

Xu, P., Duong, D.M., Seyfried, N.T., Cheng, D., Xie, Y., Robert, J., Rush, J., Hochstrasser, M., Finley, D., and Peng, J. (2009). Quantitative proteomics reveals the function of unconventional ubiquitin chains in proteasomal degradation. *Cell* *137*, 133-145.

## **Supplemental Tables**

Table S1. Strains and plasmids, Related to Figures 1 and 4-6

Table S2. SILAC based TCL quantification, Related to Figure 3

Table S3. SILAC based UbC quantification, Related to Figures 2 and 3

Table S4. Lists of KGG modified peptides, Related to Figures 2 and 3

Table S5. Potential substrates of Ubp2, Related to Figure 3

Table S6. GO analysis of Ubp2's substrates, Related to Figure 3

Table S7. Cpr1 interactome profiling, Related to Figure 6